Development of Third-Generation Gold Nanoparticles (CRISPR-AuNP) for Enhanced CRISPR Delivery to Hematopoietic Stem and Progenitor Cells

Karthikeya Srinivasa Varma Gottimukkala

A dissertation

submitted in partial fulfillment of the

requirements for the degree of

Doctor of Philosophy

University of Washington

2025

Reading committee:

Jennifer E Adair, Chair

Edus Houston Warren

Andre Lieber

Program Authorized to Offer Degree:

Department of Laboratory Medicine and Pathology

University of Washington

Abstract

Development of Third-Generation Gold Nanoparticles (CRISPR-AuNP) for Enhanced CRISPR Delivery to Hematopoietic Stem and Progenitor Cells

Karthikeya Srinivasa Varma Gottimukkala

Chair of Supervisory Committee:

Jennifer E Adair

Department of Laboratory Medicine and Pathology

Efficient CRISPR ribonucleoprotein (RNP) delivery into hematopoietic stem and progenitor cells (HSPC, CD34+) enables stable genome editing with potential for lifelong therapeutic benefits from a single intervention. However, current methods like electroporation require specialized equipment and procedures, whereas viral vectors are costly and require living cells to assemble, limiting access in research and clinical translation. Synthetic nanoparticles offer a promising alternative. We previously reported a gold-based CRISPR-AuNP nanoformulation that delivered gene editing in HSPCs, favoring Cas12a over Cas9. Here, we demonstrate that Cas9 loads poorly into this formulation. By elucidating Cas9's physicochemical interactions with AuNP surfaces, we optimized the nanoformulation by pre-forming RNP complexes in a 2nd generation CRISPR-AuNP. This formulation

demonstrated increased active Cas9 and Cas12a loading in tube but failed to deliver gene editing in primary cells in vitro. Further analysis of the CRISPR-AuNP physiochemistry with HPSC endosomes guided further optimization. Preformed RNP polyplexes were formed with thiolated poly(ethyleneimine)-poly(ethylene glycol) (PEI-PEG-SH) polymers at a 2 N/P ratio and conjugated to AuNP. This 3rd generation Cas9 CRISPR-AuNP achieved 13.23 ± 0.12% indels at the β-2-microglobulin (B2M) gene in HSPCs at a 100 pmol dose, with no observed loss in cell viability and cell entry within 6 hours. The platform's modularity extended to two additional CRISPR systems: Cas12a (15.07 ± 1.9% indels) and MG29-1 (13.39 ± 1.5% indels), highlighting its versatility. Most importantly, this nanoformulation can be assembled in a few hours at benchtop for <$70 per 1 million HSPC treated. We also demonstrate early data that this formulation can be modified with surface antibodies to facilitate active cellular targeting, with a future goal of testing these formulations in vivo for possible clinical translation. Very preliminary in vivo studies using untargeted 3rd generation Cas9 CRISPR-AuNP targeting the murine B2m gene in wild-type C57Bl6 mice showed detectable gene editing in multiple tissues with no elevated inflammatory responses or increased liver enzymes. These advancements position gold-polymeric nanoparticle hybrids as a simple, low-cost non-viral delivery system for CRISPR into HSPCs. The ability to rapidly assemble these particles with different CRISPR systems and polymers will greatly increase research access for multiple cell types.

Acknowledgments

First and foremost, I would like to thank my advisor, Dr. Jennifer E. Adair. I truly cannot imagine doing my PhD without her guidance and support. Her mentorship has shaped the way I think about science and problem-solving, and I'm grateful for the space she created, one that encouraged bold ideas while keeping one foot firmly on solid ground. I feel incredibly fortunate to have had such a rewarding graduate school experience under her leadership. It's rare to have a mentor who not only pushes science forward but also strives to leave the world better than she found it.

I would also like to sincerely thank my dissertation committee: Dr. Edus Houston Warren, Dr. Andre Lieber, Dr. Stephen Polyak, Dr. Xiaohu Gao, and Dr. Lilian Cohn. Your thoughtful feedback and insight helped refine my work in meaningful ways. I'm especially grateful to Dr. Suzie Pun, with whom I did my winter rotation. Thank you for your early encouragement and inspiration.

My appreciation goes to the M3D program, particularly Dr. Bill Mahoney and Dr. Conrad Liles for their leadership, and Megan Barker and Isabella Yasameen Shigetomi for their coordination and support. Thank you for keeping everything running so smoothly behind the scenes.

To my colleagues and lab mates at Fred Hutch and UW, thank you for fostering such a collaborative, engaging, and fun scientific environment. The camaraderie we shared made even

the most frustrating experiments manageable. I'm especially grateful to the members of the Adair Lab: Dr. Reza Shahbazi, Dr. Daniel Lane, Dr. Jack Castelli, Dr. Rachel Cunningham, Trisha Lipson, Shirley Jwa, Molly E. Cassidy, Katrina Poljakov, Dr. Heleema Malik, Dr. Grady Gastelum, Dr. Lois Bayigga, Dr. Rachel Kyeyune, Dr. Mark Enstrom, Katie Barens, Kristen Ettinger, and Janette Campos. I'd also like to thank the core facilities at Fred Hutch for their expertise and support, especially Elizabeth Jensen from the Genomics Core for her patience and consistent help.

I am deeply thankful to my family for their unwavering support and love. To my late grandfather, K.V. Narasimha Raju, your values and spirit have guided me throughout my life, and I wish you could be here to witness this milestone. To my mother, Vijaya Bharathi, and my father, Srinivasa Raju, thank you for believing in me. To my brother, Kalyan Varma, my grandmother, Vijaya Kalidindi, my sister-in-law, Nikhila Alluri, and our extended family, especially my in-laws, thank you for being part of this journey in countless meaningful ways.

To my wife, Sriya Sagi, thank you for your strength. You've seen every late night, every failed experiment, and every version of this thesis, and you stood by me through it all. I truly couldn't have done this without you.

I'm also grateful to my friends from Hyderabad and Seattle, who reminded me that life exists outside the lab. Thank you for the laughter, companionship, and for making this long journey a whole lot more fun.

Finally, I would like to thank the funding organizations that supported this research: the National Institutes of Health (NIH), the Evergreen Beyond Pilot Fund, the Bill and Melinda Gates Foundation, and the Shurl and Kay Curci Foundation. Your support made this work possible.

I dedicate this thesis to my grandfather, K.V. Narasimha Raju. He was my role model, my moral compass, and the quiet strength behind so much of who I am today. His life was a reflection of humility, resilience, and wisdom - qualities I have tried to carry with me throughout this journey. Losing him during the pandemic was a profound heartbreak, and there hasn't been a day since when I haven't wished he were here to see this moment. I hope he would have been proud. This accomplishment, though incomplete without his presence, is for him.

Table of Contents

Chapter 1: Introduction

1.1 Gene Therapy and the Emergence of CRISPR Technology

The concept of directly manipulating genetic material to treat disease has been a long-standing goal in medicine, offering the possibility of addressing the root causes of disease rather than merely managing symptoms[1]. Unlike conventional drugs that target proteins or cellular processes downstream of genetic defects, gene therapy aims to correct the underlying genetic abnormalities themselves[2]. This fundamental difference positions gene therapy as a potentially transformative approach for conditions previously considered untreatable[3]. Monogenic disorders—such as cystic fibrosis, hemophilia, and severe combined immunodeficiency (SCID)—represent logical initial targets due to their well-defined genetic etiology[4]. However, the scope has expanded considerably to include complex diseases like cancer, cardiovascular disorders, and neurodegenerative conditions[5].

The field's clinical journey began in 1990 with the first clinical trial led by the National Institutes of Health, which targeted a primary immune deficiency, adenosine deaminase severe combined immune deficiency (ADA-SCID) using an ex vivo approach: extracting the patient's hematopoietic stem and progenitor cells (HSPC; CD34+), genetically modifying them, and reintroducing them after preparative conditioning[6]. Although this initial attempt achieved modest therapeutic success, it established a critical proof-of-concept that subsequently drove the field forward[7].

The path of gene therapy development has been marked by significant challenges[8]. The 1999 death of Jesse Gelsinger from a severe immune reaction to an adenoviral vector highlighted significant safety concerns and prompted reevaluation of clinical protocols[9]. Further setbacks occurred between 2002 and 2003, when several children treated with retroviral vectors for X-linked SCID developed leukemia due to insertional mutagenesis[10]. The phenomenon of insertional mutagenesis later extended to children treated with gene therapy for Wiskott Aldrich Syndrome (WAS)[11]. These events triggered a temporary halt in multiple gene therapy trials and necessitated fundamental reassessment of vector design and safety monitoring protocols[12].

Despite these challenges, the field has demonstrated remarkable resilience and adaptive capacity. As of late 2024, there are 33 approved gene therapy products across 14 countries, signaling growing regulatory acceptance and clinical validation (ASGCT Citeline Q4 Annual Report). Particularly notable has been the recent success of gene therapies targeting hematologic disorders. The approvals of Zynteglo™ (Betibeglogene autotemcel) for β-thalassemia and Casgevy® (exa-cel) for sickle cell disease represent significant breakthroughs in treating previously intractable genetic blood disorders[13]. These therapies employ ex vivo modification of autologous HSPC, which requires mobilization of these cells out of their marrow niches, collection, purification, culture and genetic manipulation, followed by reinfusion after cytotoxic chemotherapy conditioning.

Unsurprisingly, these therapies are among the most expensive medical treatments ever developed, with Casgevy® priced at $2.2 million per treatment. This cost barrier directly relates to complex manufacturing processes, which require specialized facilities, extensive quality control, and substantial resources to produce clinical-grade material[14]. These challenges have led to commercial failures, with some authorized gene therapies being withdrawn from the market despite regulatory approval due to unsustainable economics[15].

The introduction of CRISPR-Cas9 technology as a gene editing tool in 2012 dramatically expanded gene therapy's potential by enabling precise, programmable genome editing. Originally identified in bacteria as an adaptive immune system against viral infections, CRISPR (Clustered Regularly Interspaced Short Palindromic Repeats) systems use RNA guides to direct Cas nucleases to specific DNA sequences for cleavage[16]. The pivotal innovation by Jennifer Doudna, Emmanuelle Charpentier and their teams was demonstrating the programmability of the Cas9 protein and a synthetic dual guide RNA (gRNA) for targeting double-stranded breaks in human DNA[17].

Unlike previous gene-editing technologies such as zinc finger nucleases (ZFNs) and transcription activator-like effector nucleases (TALENs), which required custom protein engineering for each genomic target, CRISPR RNA-guided nucleases can be easily programmed by simply changing the synthetic guide RNA sequence[18]. This simplicity accelerated the technology's adoption across biological research and therapeutic development, leading to remarkably swift clinical translation. In 2020, Doudna and Charpentier received the

Nobel Prize in Chemistry for their work, and in 2023, just 11 years after their discovery, the first CRISPR gene therapy product was FDA-approved for the treatment of sickle cell disease[19].

The CRISPR toolkit has expanded dramatically beyond the original Cas9 system. All CRISPR nuclease proteins contain essentially three functions: oligonucleotide binding at a cognate protospacer-adjacent motif (PAM) sequence, unwinding and/or nucleotide pairing with the guide RNA spacer, and finally, oligonucleotide cutting[20]. Cas9 utilizes a partially complementary dual RNA guide (crRNA and trRNA) to form an active ribonucleoprotein (RNP) complex, generating blunt-end double-stranded DNA breaks that lead to genomic insertions and deletions (indels)[21]. Alternative systems like Cas12a use a single guide RNA to create staggered-end cuts with a 5 bp overhang, offering advantages in thermal stability and specificity[22]. Alternative CRISPR systems identified by metagenomics can target RNA rather than DNA[23] and metagenomic analyses have identified thousands of CRISPR systems with varied capabilities[24]. More recently, several innovative CRISPR-based technologies have further expanded editing capabilities. Base editors combine a catalytically impaired Cas9 with a deaminase enzyme to convert one nucleotide to another without inducing double-strand breaks[25]. Prime editors use a Cas9 nickase fused to an engineered reverse transcriptase, enabling precise insertions, deletions, and all base-to-base conversions without requiring donor DNA templates[26]. The Programmable Addition via Site-specific Targeting Elements[27] (PASTE) system combines CRISPR-Cas and serine recombinases to enable integration of large DNA sequences, while CRISPR-associated transposase (CAST)[28] systems harness

transposases for targeted (upto 40kb) DNA insertions. Transcriptome engineering has been revolutionized through CRISPRa and CRISPRi systems, which employ catalytically inactive Cas proteins fused to transcriptional activators or repressors to precisely upregulate or downregulate gene expression without modifying the underlying DNA sequence[29]. Beyond genomic and transcriptomic modifications, CRISPR-mediated epigenome engineering, exemplified by CRISPRoff, enables targeted and heritable gene silencing through programmable deposition of epigenetic marks without permanent genetic changes[30].

Despite these remarkable advances, the therapeutic potential of CRISPR technologies remains constrained by delivery challenges—the core components must reach the nucleus of target cells in sufficient quantities to achieve meaningful editing[31]. Overcoming these delivery barriers, particularly for clinically relevant cell types like HSPC[32], remains a central focus of current research.

1.2 Hematopoietic Stem and Progenitor Cells as Prime Targets for CRISPR Therapeutics

HSPC represent particularly attractive targets for CRISPR-based gene therapy due to their unique biological properties and therapeutic potential[33]. As the precursors to all blood cell lineages, HSPCs possess remarkable self-renewal capacity and long-term repopulating ability, enabling a single successful genetic modification to propagate throughout the hematopoietic system for the patient's lifetime[34]. This "amplification effect" makes them ideal targets for treating numerous hematologic disorders, including hemoglobinopathies, primary immunodeficiencies, and certain metabolic conditions, to name a few[35].

HSPCs can be mobilized out of their bone marrow niche and into peripheral blood, collected through established clinical procedures, and manipulated ex vivo before reinfusion, creating a therapeutic workflow that has been validated through multiple approved therapies[36]. Recent clinical successes with CRISPR-edited HSPCs for sickle cell disease and β-thalassemia have demonstrated transformative therapeutic outcomes, with functional cures reported in most treated patients(Clinical Trial # NCT03655678)[37]. Additionally, advances in understanding HSPC biology have improved ex vivo culture conditions and engraftment protocols, enhancing the therapeutic potential of edited cells[38]

The transformational utility of CRISPR is underscored by the recent approval of the first gene therapy product to use CRISPR-Cas9 (exagamglogene autotemcel) for treating sickle cell

anemia[37]. This drug product consists of ex vivo CRISPR-edited autologous HSPCs. While this approach has demonstrated remarkable clinical success, there are several limitations to it's widespread availability. The ex vivo manipulation required for CRISPR editing of HSPCs is extensive, including electroporation to deliver RNP complexes and subsequent recovery from this highly toxic procedure, necessitating multi-day cellular processing[39]. These drug products are generated in a centralized manufacturing approach which requires cell products to be cryopreserved both in and out of manufacturing and is also cytotoxic to HSPC. As such, the number of HSPC which must be collected is very large (~$20x10^6$ CD34+ cells per kg of patient body weight). This complexity limits global accessibility, underscoring the need for more efficient and cost-effective CRISPR delivery into HSPCs[40].

Moreover, a foundational element of CRISPR genome engineering is the genome itself. Over the last two decades, significant efforts to increase the number and diversity of human genome sequences analyzed have revealed the geographic origins of the human species, as well as genomic loci under strong selective pressure[41]. This genetic diversity has implications for efficacy of CRISPR systems as well as their safety[42]. Therefore, it is critical to enable research of CRISPR systems in the context of local genomic diversity.

There are many components required to enable local research in genomic engineering: infrastructure and financial support for research, government policy which provides for regulation to ensure public safety and trust, and access to the research tools[43]. After 70 years in clinical use, bone marrow transplantation is still not widely adopted, and low- and middle-

income countries represent areas of neglect[44]. For research access, capacity to culture cell lines and primary cells exists where basic laboratory infrastructure is available, but access to electroporation equipment and associated reagents and materials for intracellular delivery is lacking, and ordering commercially available CRISPR proteins and gRNAs from high-income countries is expensive and difficult[45].

For clinical access worldwide, a long-term goal in the field is to develop methods for persistent HSPC genetic therapy in vivo, but these approaches face substantial challenges[1,43]. HSPCs are rare, comprising only <1% of nucleated bone marrow cells ($CD34^+CD45RA^-CD90^+$)[47,48]. While active targeting is possible, all known HSPC surface targets are also expressed elsewhere in the body, including germ line cells[49]. Freshly isolated HSPCs do not express many cell surface receptors required for active uptake by viral systems and require substantial ex vivo stimulation with media and cytokines to achieve expression of these receptors[50]. Additionally, HSPCs exhibit low translational activity complicating genetic manipulation attempts[51]. However, one feature of HSPCs advantageous for synthetic nanoparticle delivery of CRISPR cargo is a basal level of endocytosis which may or may not rely on cell surface receptors[52]. Recently it was demonstrated that delivery of CRISPR into unstimulated HSPC ex vivo resulted in increased safety and fitness of these cells[53]. Altogether, the development of simple, affordable technology which can deliver CRISPR to living hematopoietic cells without the need for specialized equipment would be transformative for global research and clinical translation.

1.3 Current CRISPR Delivery Methods and Their Limitations

The therapeutic potential of CRISPR technology depends on developing effective delivery strategies for its core components: Cas9 (or other nuclease) protein, guide RNA (gRNA), and occasionally donor DNA. Both viral and non-viral delivery methods have emerged as viable strategies, each with distinct advantages and limitations that influence their suitability for different applications, particularly for HSPCs[54,55].

1.3.1 Viral Vector Delivery Systems

Viral vectors represent the most clinically mature platforms for gene therapy and CRISPR delivery, leveraging virus's natural ability to introduce genetic material into cells[5]. Lentiviruses, predominantly derived from human immunodeficiency virus type 1 (HIV-1), are widely used for ex vivo CRISPR delivery due to their ability to transduce both dividing and non-dividing cells[56]. These retroviruses integrate their genetic payload into the host genome, enabling sustained expression of Cas9 and gRNA[2]. However, this integration introduces insertional mutagenesis risks, partly mitigated by self-inactivating designs[10]. Their limited packaging capacity (~8–10 kb) struggles to accommodate the ~4.2 kb SpCas9, often requiring alternative orthologs of Cas9[57]. And finally, integration results in permanent expression of CRISPR components, which is associated with increased risk of genotoxicity[58]. Integration-deficient lentiviral vectors have been described and used for CRISPR delivery[59].

Adeno-associated viruses (AAVs) have become preferred vectors for in vivo CRISPR delivery due to their favorable safety profile and tissue-specific tropisms[60]. Unlike lentiviruses, AAVs

persist primarily as episomal DNA, reducing insertional mutagenesis risk, though their small packaging capacity (~4.7 kb) necessitates dual-vector systems for full CRISPR constructs[61]. A common strategy employs one AAV to deliver Cas9 and another for the guide RNA(s), which requires co-infection of target cells with both vectors, reducing overall efficiency[62]. Pre-existing immunity to AAV capsids in 30-70% of humans can substantially reduce transduction efficiency and provoke immune responses, requiring serotype optimization or immunosuppression, which increases clinical complexity[63].

Helper-dependent adenoviruses (HD-Ads), pioneered in part by Lieber and colleagues, represent an advanced viral vector design with all viral coding sequences removed except the inverted terminal repeats. This gutless approach significantly increases payload capacity—a critical advantage for CRISPR applications—while potentially reducing immunogenicity compared to conventional vectors[64]. This technology has been applied to deliver CRISPR and other transgenes in vivo following re-targeting of the HDAd to hematopoietic stem cells[65]. Despite their advantages, HD-Ads face challenges in large-scale production and purification due to the requirement for helper viruses, which can complicate manufacturing and increase costs for clinical applications[66].

For HSPC applications, viral delivery poses challenges due to the cells' limited transcriptional activity and natural antiviral responses that can compromise cellular fitness[51]. Only integrating vectors provide durable therapeutic effects to this cell type, as transgene expression must persist through cell division and differentiation[4]. While this strategy has led to successful

treatments, untargeted integration presents the risk of abnormal gene expression and oncogenic mutations, as seen in early trials for X-SCID and WAS gene therapies wherein a subset of patients developed leukemia[67].

However, for all viral approaches, a major disadvantage is that viral particles must be assembled by living cells. All components for the viral particle must be transferred into a producer cell line and are not always conducive to maintaining a working cell bank, relying instead on transient transfection of viral components for each individual manufacturing run[68] To avoid the risk of an engineered viral particle for delivery recombining with a naturally occurring virus, engineered viral components are separated into individual plasmids[69]. Once all viral components are delivered into the cells, viral particles must be collected from media over time and purified from cellular components and residual manufacturing reagents such as excipient plasmid DNA encoding viral transgenes. This often results in low yields of functional viral particles. As such, viral production requires specialized facilities and expertise, contributing to the high cost of viral vector-based therapies, which can exceed $1 million per patient[70]. These limitations underscore the value of scalable, synthetic delivery modalities. However, whereas synthetic approaches are easier to make, viruses have evolved to traffic into cells and nuclei. Thus, a major obstacle for synthetic delivery is engineering the ability to enter cells and traffic to the nucleus for functional activity.

1.3.2 Electroporation and Other Non-Viral Approaches

Electroporation, the current standard for clinical HSPC editing including the approved Casgevy® therapy, achieves high efficiency (40-80%) by using electrical pulses to deliver pre-formed CRISPR RNP complexes directly to cells[39]. While electroporation temporarily opens both the plasma and nuclear membranes, trafficking to the nucleus is facilitated by the addition of nuclear localization signal (NLS) peptides to the Cas9 nuclease protein[71]. The approach benefits from enabling immediate editing activity without requiring transcription or translation and limiting the duration of nuclease expression to reduce off-target effects[72]. However, this approach induces significant cellular stress and cytotoxicity, requires specialized equipment and reagents, and necessitates complex multi-day processing that limits global accessibility[33].

Non-viral delivery systems for CRISPR are gaining increasing attention for their potential to overcome the safety, capacity, and production challenges associated with viral vectors[73]. These approaches enable delivery of CRISPR components in diverse formats—DNA, mRNA, or ribonucleoprotein (RNP) complexes—offering versatility and reduced immunogenicity compared to viral methods[54].

Lipid nanoparticles (LNPs) have emerged as a prominent in vivo delivery platform, with proven efficacy in mRNA vaccine technologies most notably for the prevention of SARS-CoV2 infection [74]. Composed of ionizable lipids, helper lipids, cholesterol, and PEG-lipids, LNPs encapsulate CRISPR cargo and promote cellular uptake, achieving particular success in targeting hepatocytes[75]. The ionizable lipids exhibit pH-dependent charge properties,

becoming cationic in the acidic endosomal environment to facilitate membrane disruption and endosomal escape[76]. However, as LNP systems primarily rely on oligonucleotide delivery, they suffer directly from the low translational activity of in situ HSPCs, requiring targeting, large doses, and optimization of the therapeutic window across patients[51].

Engineered virus-like particles (eVLPs) represent an emerging approach that aims to combine the delivery efficiency of viruses with the safety profile of synthetic systems[77]. These nanoparticles mimic the structural features of viruses that facilitate cellular entry while eliminating infectious components[78]. A notable advantage of eVLPs is their ability to package intact RNP complexes, avoiding the size limitations of viral vectors. However, eVLP production remains challenging, requiring complex protein engineering to enable RNP packaging into the viral particle and still depends on living cells for assembly, often resulting in heterogeneous particle populations with variable loading capacity[78]. More recently, both eVLPs and LNPs capable of carrying RNP cargo have been described, but to date have not been evaluated for efficient in vivo delivery to HSPCs without toxicity[79].

Cell-penetrating peptides (CPPs) have recently been adapted for CRISPR delivery through peptide-enabled RNP delivery for CRISPR editing (PERC) [80]. This approach uses positively charged membrane-active peptides added to the culture along with Cas nucleases, enabling cellular uptake without additional carriers. While showing promise, current formulations still fall short of the editing efficiency observed following electroporation in HSPCs, face challenges in achieving consistent performance across different cell donors and targets, and can be associated with toxicity[81].

1.4 Gold-Based Nanoparticles for CRISPR Delivery

Gold nanoparticle (AuNP) systems offer several intrinsic advantages as delivery vehicles, including precise size control, stability under physiological conditions, minimal toxicity, and unique optical properties enabling tracking through various imaging modalities[82,83,84].

CRISPR-gold, developed by Murthy group, represents a significant advancement for in vivo gene editing applications. This system consists of gold nanoparticles surface-functionalized with thiolated DNA, which are subsequently complexed with Cas9 RNP and donor DNA templates[85]. The particles are coated with an endosomal disruptive polymer that enhances cellular uptake and facilitates endosomal escape following internalization. Murthy's group has demonstrated the efficacy of CRISPR-gold across multiple cell types and disease models, notably achieving correction of the dystrophin gene in mouse models of Duchenne muscular dystrophy[85].

Rotello and colleagues have developed complementary AuNP-based delivery systems utilizing arginine-functionalized gold nanoparticles[86]. These systems leverage controlled surface chemistry to optimize the complexation and delivery of Cas9 RNP. The arginine functionalization confers both positive charge for cellular uptake and membrane-active properties that facilitate endosomal escape[87].

We previously described a first-generation gold-based CRISPR-AuNP nanoformulation capable of carrying CRISPR systems as RNP without the need for nuclease engineering[82]. In this system, Cas9 or Cas12a RNP were anchored through thiol modification of gRNA,

forming a self-assembled monolayer on the AuNP core surface. After gRNA monolayer formation, nuclease was added and allowed to associate, forming tethered RNP on the AuNP surface. These particles were electrostatically coated in polyethyleneimine (PEI), an endosomal disrupting polymer with net positive charge. This positively charged layer then permitted electrostatic loading of 80nt single-stranded DNA oligos to serve as templates for HDR. Advantages of this nanoformulation included rapid assembly, no observable toxicity to primary human HSPCs in vitro, and retained fitness of edited HSPCs in vivo in a mouse xenograft model of human hematopoiesis[82]. We observed integration of DNA templates with both nucleases, but levels were higher for Cas12a than Cas9. Indel levels with Cas9 were comparable to those of Cas12a, which was unexpected given Cas9's typically higher efficiency, and neither nuclease achieved editing levels considered therapeutic (≥10% of HSPCs)[88], leaving room for improvement. In further unpublished studies, these 1st generation CRISPR-AuNP were administered to humanized NSG mice via intravenous injection after HSPC mobilization with filgrastim and plerixafor. Injections were well-tolerated and low level gene editing was observed in circulating WBCs at 2 weeks after administration, but not at any other time point during the study which lasted 16 weeks. Moreover, the only edits observed were indels, suggesting that DNA cargo may have been separated from CRISPR-cargo under physiological conditions. At the time of these studies, prime editors emerged, suggesting that DNA cargo may not be required if Cas9-based CRISPR loading could be optimized.

This thesis investigates the physicochemical properties of Cas9 and its interactions with gold nanoparticle surfaces to enhance CRISPR-AuNP loading and activity in primary human

HSPCs. The goal is to develop a CRISPR-AuNP platform that offers several advantages over current delivery methods:

1. Simplicity and Rapid Assembly: Developing a system that can be assembled in less than a day with commercially available materials, requiring no advanced engineering.
2. Cost-Effectiveness: A delivery platform substantially less expensive than viral vector or electroporation approaches.
3. Versatility Across CRISPR Systems: Establishing a modular design capable of accommodating various CRISPR nucleases and next-generation editing tools.
4. Maintained Cell Viability: Ensuring the delivery method preserves HSPC viability and fitness.
5. Therapeutic Editing Efficiency: Achieving indel frequencies above 10%[88], generally considered the minimum threshold for therapeutic applications.

The research presented in subsequent chapters details the systematic optimization of CRISPR-AuNP formulations, from identifying key limitations in the 1st generation system to developing an improved 3rd generation platform. Chapter 2 focuses on elucidating and addressing the physicochemical factors affecting Cas9 loading, cellular uptake, and endosomal escape in a system capable of delivering therapeutically relevant editing levels in HSPCs without compromising viability. Chapter 3 expands on these findings to position the technology within the broader landscape of gene editing delivery systems, exploring antibody-mediated targeting for enhanced specificity and preliminary in vivo applications.

By advancing non-viral CRISPR delivery technology, this work aims to increase the accessibility of gene editing tools for research and therapeutic applications, potentially expanding the transformative benefits of precision genetic medicines to regions and populations with limited access to specialized facilities and equipment[70].

Chapter 2: Optimization of CRISPR-AuNP

We previously reported a 1st generation gold-based CRISPR-AuNP capable of delivering RNP complexes to HSPCs without requiring nuclease engineering[82]. Initial characterization of this platform demonstrated anchoring of CRISPR ribonucleoproteins to AuNP surfaces via thiol-modified guide RNAs, with a cationic polyethyleneimine (PEI) coating providing endosomal disruption capability[91]. Although this first-generation system established proof-of-concept for nanoparticle-mediated delivery to HSPCs without compromising cellular viability, functional assessment revealed editing efficiencies below the threshold typically considered necessary for therapeutic applications (≥10% edited cells). These preliminary findings highlighted the need for mechanistic investigation into factors limiting CRISPR activity when delivered via nanoparticle carriers.

Notably, the first-generation system showed unexpectedly similar editing efficiencies for both Cas9 and Cas12a, despite Cas9's typically superior performance in direct comparisons[92]. This observation suggested suboptimal loading or functionality of Cas9 on the nanoparticle surface, potentially due to destabilization of the dual RNA guide (crRNA and tracrRNA) under the synthetic conditions. Additionally, the PEI coating strategy, while effective for facilitating cellular uptake, may have been insufficient for optimal endosomal escape in the challenging context of primary HSPCs. Electrostatic binding of PEI and DNA in these first-generation particles also risks separation of these cargo from the base particle and the covalently anchored CRISPR cargo.

In this study, we systematically investigated the physicochemical interactions between CRISPR-Cas9 RNPs and gold nanoparticle surfaces to enhance loading, stability, and delivery efficiency.

Results

B-2-microglobulin (B2M) Knockdown as a Model to Compare Different CRISPR-AuNP Formulations

While our previous studies targeted the CCR5 (Chemokine Receptor 5) or **γ**-globin promoter loci for gene editing, these sites do not permit rapid evaluation of gene editing at both the gDNA and protein level. To allow genomic and protein level quantification of gene editing, the human B2M gene was selected. B2M is a cell surface, membrane-expressed protein in nucleated cells. If gene editing results in indels which compromise protein folding, loss of cell surface protein expression is observed, permitting rapid evaluation by flow cytometry in living cells. All possible Cas9 gRNAs (>100) were identified within human B2M exons based on human genome assembly GRCh38/hg38, then winnowed using Chen W et. al.'s[93] method for determining a target genomic site's predicted likelihood to introduce ≥3bp deletions following a CRISPR-induced double-strand DNA break, with the top 20 selected for RNP screening. Cas9 RNP complexes containing each of the top 20 candidate gRNA were electroporated into Jurkat cells and evaluated by flow cytometry for loss of cell surface B2M protein and DNA sequencing to determine editing levels in genomic DNA (gDNA) (Figure. 1). Although the gRNA efficiency was tested in the Jurkat cell line, this approach enabled identification of the

most effective gRNA, which can be used in future studies evaluating nanoparticle delivery in CD34+ cells targeting B2M. Of the gRNAs tested, Cas9 gRNA 4, targeting exon 2 in a region vital to B2M interaction with major histocompatibility class (MHC) 1 protein, was associated with loss of B2M expression in 54.7 ± 20.6% of cells and was associated with 65.0 ± 24.0% gene editing measured by CRISPRESSO tool[94] (defined by altered DNA sequence reads relative to the cut site vs total reads; n= 3 technical replicates; values represented as mean ± standard deviation), following electroporation of 100 pmol RNP. Other Cas9 gRNAs which significantly suppressed B2M surface expression targeted either the promoter region or exons 1 and 2. While high gene editing levels were observed in exons 3 and 4, these were associated with little to no knockdown of B2M protein expressed on the cell surface (Figure. 1). gRNA 4 was selected for its high B2M protein knockdown to facilitate further CRISPR-AuNP development.

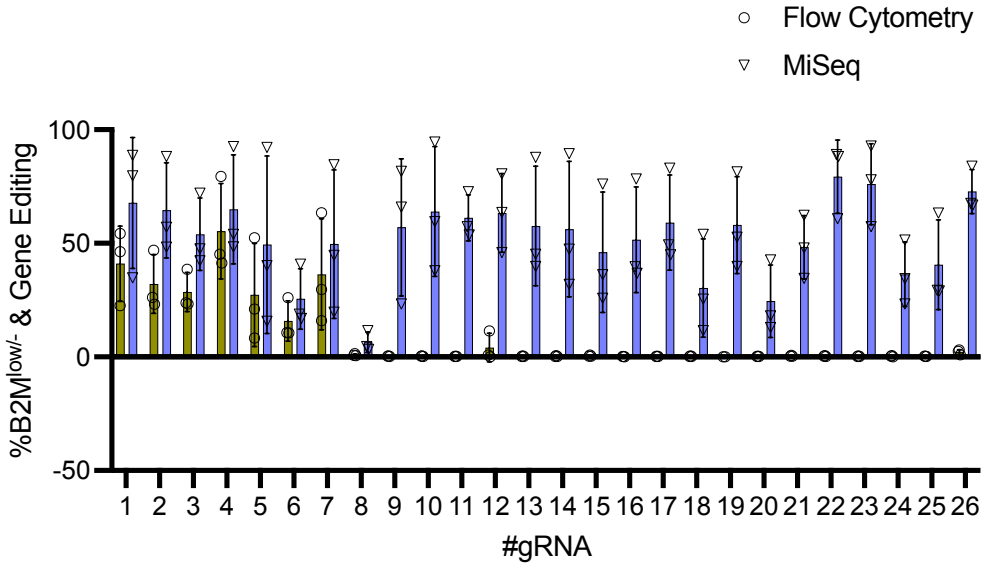

Figure. 1 | gRNA 4 targeting B2M exon 2 demonstrates highest editing efficiency in Jurkat cell.

Flow cytometry and MiSeq sequencing data show B2M editing in Jurkat cells electroporated with Cas9 RNP complexes containing selected gRNAs targeting the B2M gene using the Neon Electroporation System (n = 3 independent experiments). Bar graphs display the percentage of $B2M^{low/-}$ cells determined by flow cytometry and the percentage of edited reads (insertions/deletions or substitutions within 40 bp of the predicted cut site) quantified by MiSeq sequencing with CRISPRESSO analysis for each gRNA.

We next determined the RNP dose required to achieve effective editing in primary human HSPC. A range of RNP was electroporated into HSPCs and compared against mock treatment. A dose of 100 pmol RNP demonstrated the highest stable gene editing at 43.9 ± 17.9% $B2M^{low/-}$ cells by flow cytometry and 47.8 ± 15.3% frequency of edited reads by DNA sequencing, while a dose of 30 pmol RNP resulted in the lowest, yet statistically significant level of gene editing across donors (n=3) (Figure. 2). The 100 pmol dose was selected for CRISPR-AuNP study doses.

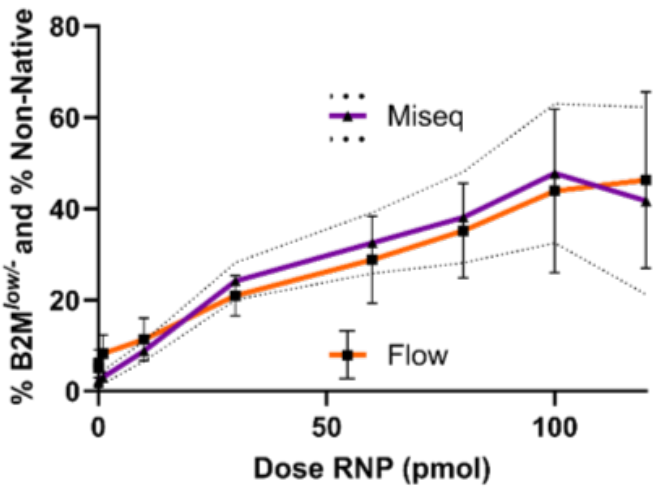

Figure. 2 | 100 pmol Cas9 RNP dose achieves maximal B2M editing in primary human HSPCs with plateau at higher doses

Dose-response curve showing gene editing efficiency in primary human HSPCs from three independent donors (n=3) electroporated with increasing doses (0-125 pmol) of Cas9 RNP targeting the B2M gene (gRNA #4) using the Neon Electroporation System. Orange line with squares represents the percentage of $B2M^{low/-}$ cells determined by flow cytometry, while purple line with circles shows the percentage of edited DNA sequence reads quantified by sequencing with CRISPRESSO analysis. Dotted gray lines indicate standard error of the mean (SEM) for MiSeq data.

Poor Cas9 Nuclease Loading on 1st generation CRISPR-AuNP

Across many studies by different groups, Cas9 demonstrates more efficient indel formation relative to Cas12a[92]. Comparatively, the CRISPR-AuNP developed by Shahbazi et.al.[82], here in referred to as 1st generation CRISPR-AuNP (Figure. 3) resulted in similar, low gene editing

efficiency with Cas12a or Cas9 in HSPC in vitro. Lower than expected Cas9 activity was originally attributed to lower efficacy of the gRNA designed to target the CCR5 gene. Gene editing at this gene does not result in measurable protein differences, lending to DNA sequencing being the only measure to efficacy. To address this, we applied B2M RNP for these studies. We synthesized 1st generation CRISPR-AuNP targeting B2M, but observed no detectable gene editing in treated HSPC (Figure. 4A). We previously demonstrated that 1st generation CRISPR-AuNP can enter primary human HPSC by confocal microscopy wherein trRNA and HDT cargo were fluorescently modified. However, this study did not track nuclease protein or functional RNP activity.

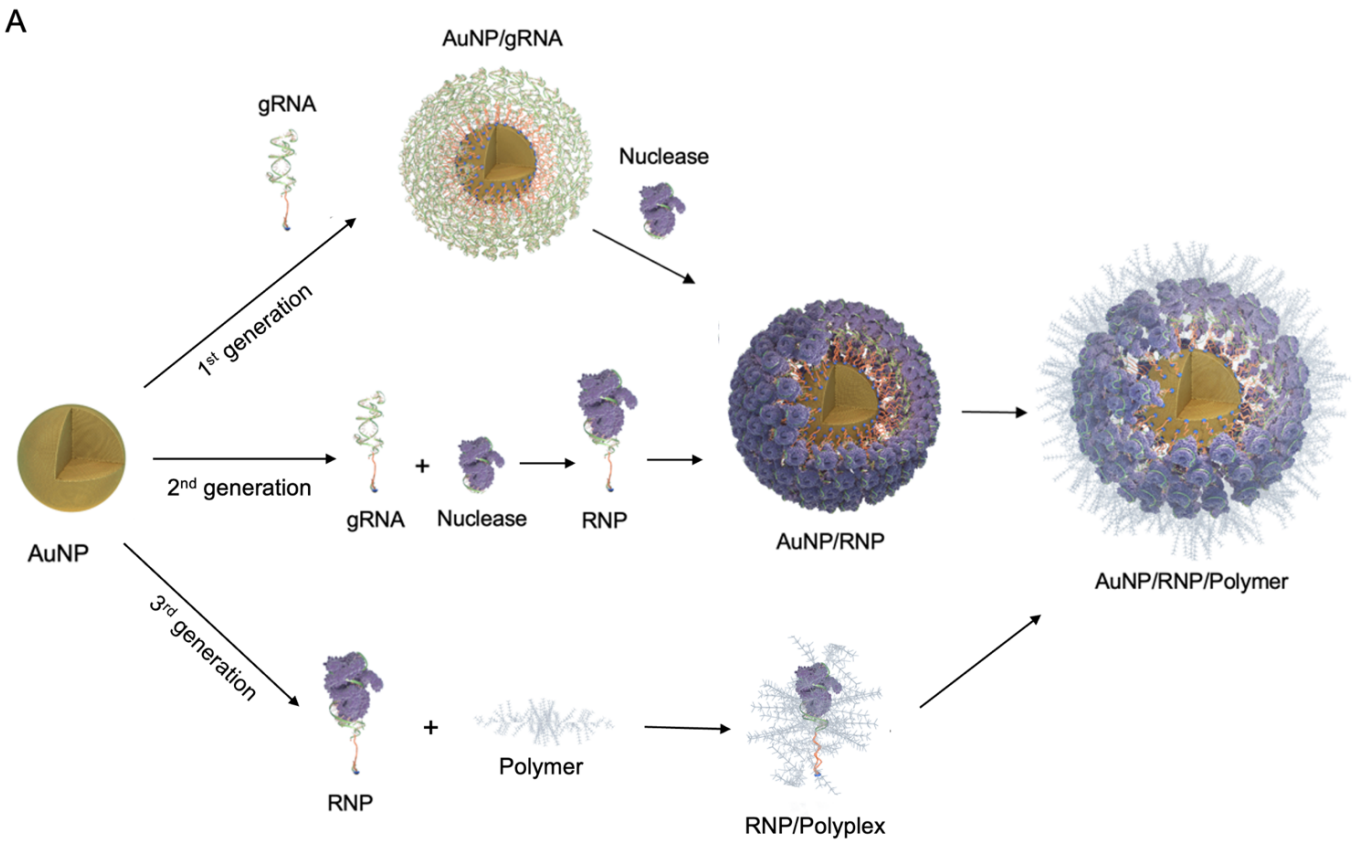

Figure. 3 | Schematic of CRISPR-AuNP synthesis across generations

Illustration of the stepwise development of different generations of CRISPR-AuNP. The 1st generation approach involves sequential attachment of thiolated gRNA to the gold surface followed by Cas9 association and PEI coating. The 2nd generation system uses pre-formed RNP complexes conjugated to gold at optimized pH with thiolated PEG-PEI coating. The 3rd generation approach incorporates pre-formed RNP-polymer polyplexes at optimized N/P ratios before conjugation to gold cores, resulting in more stable particles with enhanced delivery efficiency.

To validate if RNP is present in 1st generation CRISPR-AuNP, we performed direct measurement of Cas9 protein by SDS-PAGE densitometry after RNP is released from AuNP core by β-mercaptoethanol (BME)[95]. This revealed undetectable levels of Cas9 nuclease, but detectable levels of Cas12a on 1st generation CRISPR-AuNP (Figure. 5). Cas9 nuclease loading relies on thiolated crRNA-trRNA duplex (gRNA) anchored to the AuNP surface in 1st generation CRISPR-AuNP. As previously reported, the modifications required to adapt RNA to attach to the gold surface requires a 12-unit oligoethylene glycol (OEG) spacer to buffer electrostatic repulsion between RNA molecules in addition to a thiol anchor. This permits full saturation of the AuNP surface with RNA, stabilizing the particles in solution. However, these modifications were at the time not commercially available to form Cas9's longer single gRNA, requiring the use of crRNA/trRNA duplex. The duplex is itself held together by a low energy, 10 bp of RNP with a melting point of 28º C in our formulation conditions. Under the low pH conditions required to conjugate the negatively charged gRNA to the negatively charged

AuNP surface, the melting point is further reduced. We hypothesized that these low pH conditions could destabilize the crRNA/trRNA duplex, which would compromise nuclease interactions requiring full duplex which are structurally stabilized by trRNA. We labeled Cas9 crRNA with ATTO488 for detection simultaneously with ATTO550 labeled trRNA to confirm binding of both components. 1st generation CRISPR-AuNP were assembled up to the gRNA monolayer stage with co-labeled crRNA/trRNA. Fluorescence measurements revealed only 9.2 ± 4.1 trRNA/AuNP core, but 58.1 ± 8.5 crRNA/AuNP core, suggesting an unbalanced, trRNA-depleted surface (Figure. 4B).

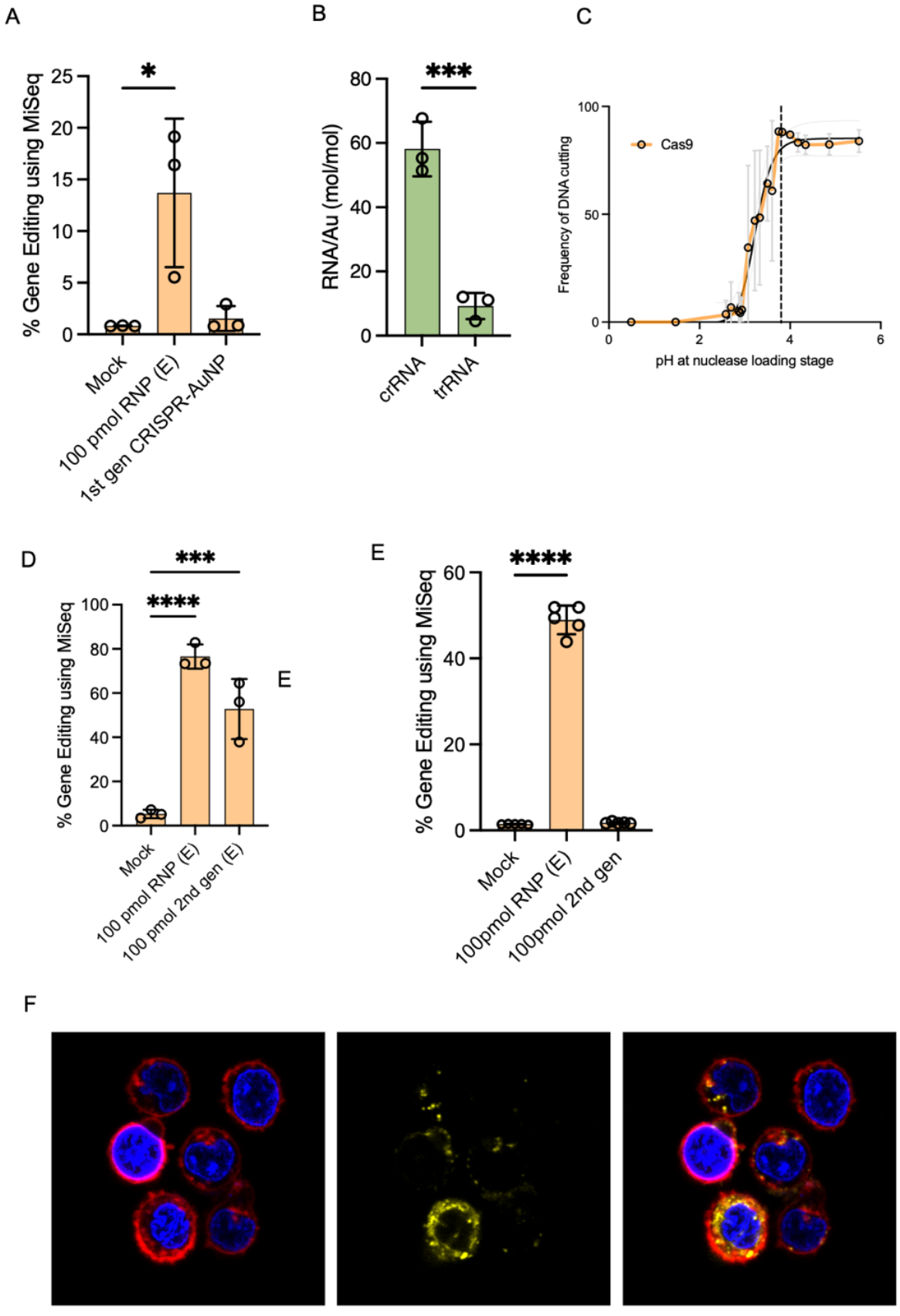
A
% Gene Editing using MiSeq
25
20
15
10
5
0
*
Mock
100 pmol RNP (E)
1st gen CRISPR-AuNP
B
RNA/Au (mol/mol)
80
60
40
20
0
***
crRNA
trRNA
C
Frequency of DNA cutting
100
50
0
Cas9
0
2
4
6
pH at nuclease loading stage
D
% Gene Editing using MiSeq
100
80
60
40
20
0
***
****
Mock
100 pmol RNP (E)
100 pmol 2nd gen (E)
E
% Gene Editing using MiSeq
60
40
20
0
****
Mock
100pmol RNP (E)
100pmol 2nd gen
F

Figure. 4 | 2nd generation CRISPR-AuNP display favorable loading and nanoformulation characteristics but fail to escape HSPC endosomes.

A) Indel frequency at the B2M gene in CD34+ HSPCs treated with 1st generation CRISPR-AuNP (100 pmol RNP dose) or untreated controls. Data represent mean ± s.d. (n=3 biological replicates). B) Fluorescence quantification of ATTO550-tracrRNA and ATTO488-crRNA loading on 1st generation CRISPR-AuNP showing unbalanced distribution (9.2 ± 4.1 tracrRNA vs. 58.1 ± 8.5 crRNA per AuNP core; mean ± s.d., n=3). C) In-tube dsDNA cutting assay measuring Cas9 RNP activity after conjugation to AuNP at pH 2.5–7.0. Peak activity observed at pH 3.8. Data represent mean ± s.d. (n=3 technical replicates). D) Indel frequency in CD34+ HSPCs electroporated with 2nd generation CRISPR-AuNP (52.7 ± 13.5%) or free Cas9 RNP (76.5 ± 5.5%) at 100 pmol dose. Data represent mean ± s.d. (n=3). E) Indel frequency in CD34+ HSPCs treated with fully assembled 2nd generation CRISPR-AuNP (100 pmol RNP dose). Data represent mean ± s.d. (n=5). F) Confocal microscopy of CD34+ HSPCs treated with 2nd generation CRISPR-AuNP containing ATTO550-tracrRNA (yellow). Plasma membrane stained with CellMask Deep Red (red), nucleus with NucBlue (blue). Scale bar, 10 μm.

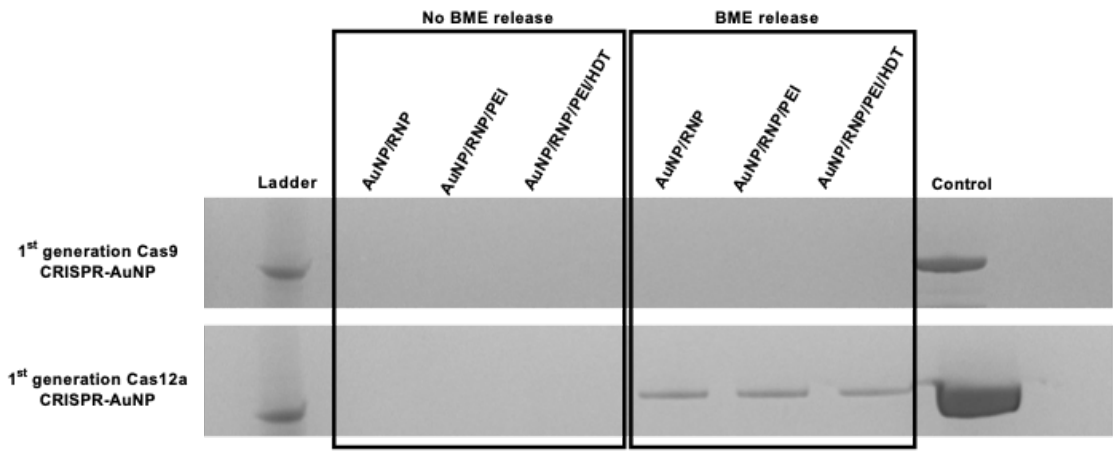

Figure. 5 | SDS-PAGE analysis confirms Cas12a loading but not Cas9 on 1st generation CRISPR-AuNPs.

SDS-PAGE images show protein released from 1st generation CRISPR-AuNPs synthesized with Cas9 or Cas12a, treated with 5 mM BME in DPBS overnight at 4°C to cleave thiol linkages. Detectable bands appear for Cas12a RNP (~160 kDa), but not for Cas9 RNP (~163 kDa), confirming differential loading efficiency between nucleases. Visible ladder band is 130 kDa MW.

Recovering Stable and Active Cas9 Loading on AuNP via Preformed RNP Complexes

1st generation CRISPR-AuNP were subjected to a pH of 3.0 during the first stage of synthesis (gRNA loading), which is not suitable for preserving nuclease structure and activity. Research by O'reilly et al[96]. demonstrated an increased Cas9 nuclease melting temperature after addition of duplexed RNA, indicating enhanced stability of the RNP over duplex gRNA or nuclease

alone. We hypothesized that this increased stability would increase the binding stability of the duplex gRNA as well as restricting the AuNP core surface to only binding full RNP complex, instead of forming an RNA monolayer. However, a preformed Cas9 RNP also carries a negative charge of -5 mV to -10 mV, even when the OEG-spacer-modified gRNA is used. This necessitates a pH <7 to permit RNP approach to the negatively charged AuNP core surface. Given that any pH lower than physiological risks protein denaturation, we investigated the activity of Cas9 RNP from neutral pH to pH 2.5, where denaturation is assured, using an in-tube dsDNA cutting assay. After preforming RNP and coating AuNP at various pH levels, assembled RNP-AuNP were purified using centrifugation, BME treated and RNP activity was measured as a function of the quantity of cutting of a targeted dsDNA PCR amplicon encoding the desired target PAM and gRNA complimentary sequence. Peak DNA cutting activity for Cas9, corresponding to a combination of RNP binding to AuNP and pH resistance, was pH 3.8 (Figure. 4C). We termed this approach of directly conjugating preformed RNP to AuNP as 2nd generation CRISPR-AuNP. As a final confirmation of activity, we electroporated 2nd generation CRISPR-AuNP into HSPC to simulate successful intracellular delivery, as compared to electroporation of free RNP. Electroporation of 2nd generation CRISPR-AuNP at the AuNP/RNP stage, using a 100 pmol dose quantified by SDS-PAGE densitometry (Figure. 6), was compared to electroporation of a 100 pmol RNP dose. Gene editing efficiency, measured via DNA sequencing, was 52.7 ± 13.5% for electroporated 2nd generation CRISPR-AuNP, whereas electroporation of free RNP achieved 76.5 ± 5.5% editing in HSPCs (Figure. 4D). These results show that 2nd generation CRISPR-AuNP retains sufficient active RNP to evaluate gene editing using the B2M model.

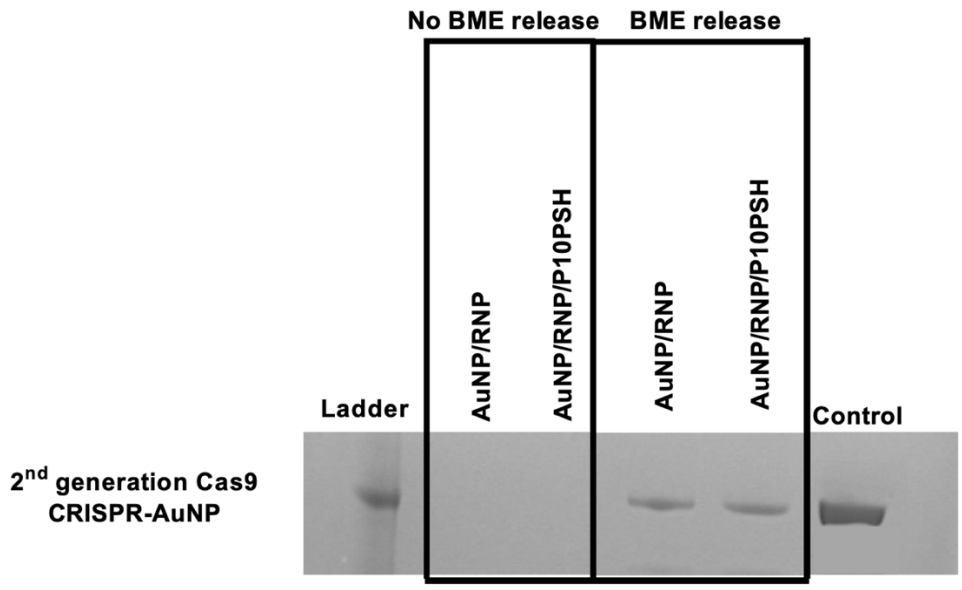

Figure 6 | SDS-PAGE analysis confirms successful Cas9 loading onto 2nd generation CRISPR-AuNPs.

SDS-PAGE images show protein released from 2nd generation CRISPR-AuNPs at various stages, treated with 5 mM BME in DPBS overnight at 4°C to cleave thiol linkages. Control band is Cas9 RNP (~163 kDa). Visible ladder band is 130 kDa MW.

2nd generation RNP-AuNP Coating with Cationic Polymers

Endosomal escape of the 1st generation CRISPR-AuNP was mediated by cationic polymer electrostatically coated onto AuNP after RNP loading[82]. The polymer used in 1st generation CRISPR-AuNP was a low molecular weight (MW, 2K), branched chain PEI. This low MW

PEI is less toxic to mammalian cells than longer linear chain or larger MW PEI[91]. Encapsulation of 1st generation CRISPR-AuNP was mediated by electrostatic attraction between the cationic PEI and the negatively charged AuNP/RNP complex of -27 mV. However, addition of 2K MW branched PEI to 2nd generation RNP-AuNP resulted in particle aggregation to >1 μm hydrodynamic diameter measured by dynamic light scattering (DLS) (Figure. 7).

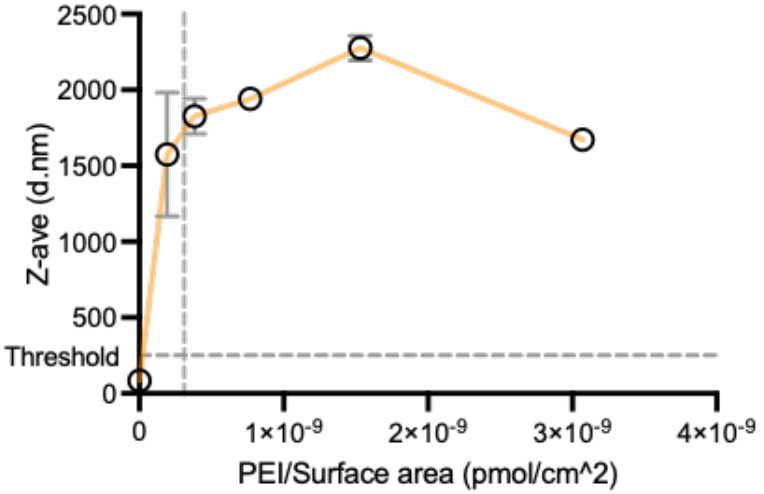

Figure. 7 | 2nd generation CRISPR-AuNPs aggregate during PEI encapsulation, limiting colloidal stability.

Plot shows Z-average hydrodynamic diameter of 2nd generation CRISPR-AuNPs encapsulated with branched PEI (2k MW) at increasing PEI-to-AuNP surface area ratios, measured by DLS. CRISPR-AuNPs are synthesized to the AuRNP stage and coated with PEI. Particle size exceeds 1,000 nm at higher ratios.

One mechanism to increase colloidal stability is with polyethylene glycol (PEGylation)[97]. To test this, PEI was 10% grafted with thiolated polyethylene glycol (PEG) to form 2k-PEI-10g-2k-PEG-SH (P10PSH). We hypothesized that PEG-thiol could covalently anchor to available AuNP core surface providing stability. Adding 32 mg of P10PSH per 40 ug of AuNP/RNP complex by AuNP mass resulted in stable CRISPR-AuNP by DLS measuring 131.7 ± 3.5 nm in hydrodynamic diameter (Figure. 8) with a polydispersity index (PdI) of 0.223 ± 0.027 and zeta potential of -0.6 ± 1.1 mV (n=3 technical replicates). Additional copolymer resulted in no additional size or charge changes, indicating saturation of coating. Fully formed 2nd generation CRISPR-AuNP demonstrated 39.6 ± 7.0 Cas9 RNP complexes per AuNP core by SDS-PAGE when released with BME, and in-tube cutting assay demonstrated successful fragmentation of targeted dsDNA (Figure. 9), indicating active RNP loading after formulation and purification to remove unbound excess.

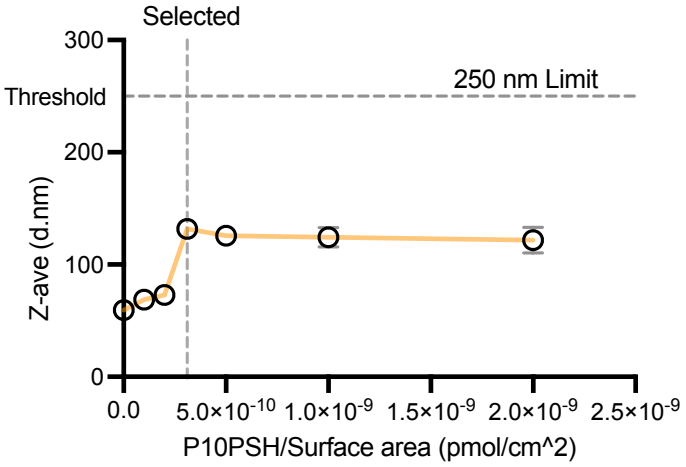

Figure. 8 | Thiolated PEG-PEI copolymer (P10PSH) provides stability to 2nd generation CRISPR-AuNPs.

DLS analysis of 2nd generation CRISPR-AuNPs following encapsulation with P10PSH (2k MW PEI grafted with 10% 2k MW PEG-SH). Particles were synthesized to the AuRNP stage, coated with P10PSH, and analyzed by DLS.

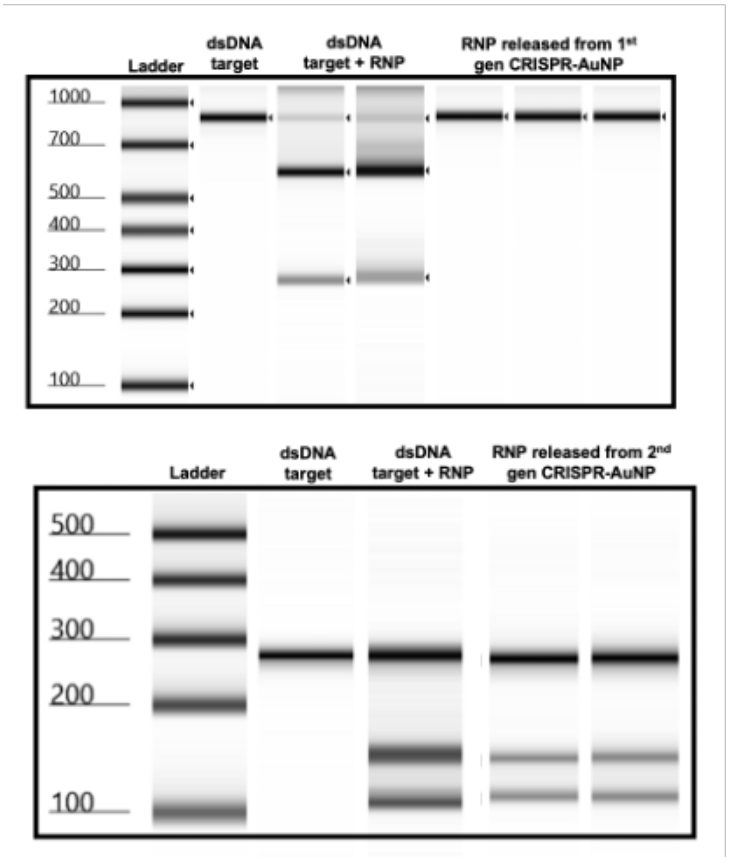

Figure. 9 | 2nd generation Cas9 CRISPR-AuNPs have functionally active Cas9 RNP on their surface.

TapeStation gel images showing in-tube DNA cutting assay using Cas9 RNP released from 1st and 2nd generation CRISPR-AuNPs. Distinct cleavage bands appear from 2nd generation Cas9 CRISPR-AuNP, while no cleavage is detected from 1st generation Cas9 CRISPR-AuNP.

2nd generation CRISPR-AuNP fail to deliver Cas9 to the nucleus

We treated HSPCs with a dose of fully assembled 2nd generation CRISPR-AuNP equivalently to 100pmol RNP to evaluate gene editing efficiency at the B2M gene 72 hours post-treatment. To achieve this dose, the corresponding 2nd generation CRISPR-AuNP dose was calculated based on the amount of RNP bound to the AuNP core, as determined by SDS-PAGE. This treatment resulted in a non-statistically significant trend in B2M gene editing, falling below the expected value given the increased RNP loading density (Figure. 4E). We further investigated the uptake mechanism of 2nd generation CRISPR-AuNP by labeling with ATTO550-trRNA, treating HSPCs and imaging via confocal microscopy. HSPCs exhibited punctate fluorescence within the cytoplasm, consistent with endosomal internalization with no diffuse cytoplasmic fluorescence observed, suggesting endosomal entrapment (Figure. 4F). Interestingly, we also observed globular staining of HSPCs with the membrane dye following treatment with 1st generation CRISPR-AuNP[82]. Since PEI polymer can bind the membrane dye used, this suggests that electrostatically bound PEI sloughs off of 1st generation CRISPR-AuNP when added to HSPC in media. Together with gene editing data, these findings indicate that the alternative copolymers used to stabilize 2nd generation CRISPR-AuNP are insufficient to mediate effective endosomal escape in primary HSPCs, and that gene editing observed after treatment with 1st generation CRISPR-AuNP may have resulted from polyplex mediated intracellular delivery, rather than intracellular trafficking of intact particles as shown by the confocal imaging[82].

Optimization of co-polymer dose results in HSPC gene editing

Since the co-polymer facilitates endosomal escape[98], we first sought to determine whether co-polymer dose on 2nd generation CRISPR-AuNP was sufficient for effective RNP delivery into HSPCs. To assess this, we formulated various amine to phosphate (N/P) ratios of P10PSH polyplexes with RNP targeting the B2M gene.

Characterization of these polyplexes by DLS revealed instability over time across all N/P ratios, with PdI values ranging from 0.3 to 1.0 (threshold < 0.3) and hydrodynamic particle diameters between 50–150 nm. Successful electrostatic binding of the co-polymer to the negatively charged RNP complexes was confirmed by a zeta potential shift from negative to positive, which plateaued at N/P > 8 (Figure. 10A).

We then treated HSPC with these polyplexes and measured the B2M knock down efficiency using flow cytometry and gene editing by DNA sequencing. Flow cytometry revealed increasing levels of B2M knockdown from N/P 2 to N/P 8, with a subsequent decrease up to N/P 64 (Figure. 10B). This trend was mirrored in indel percentages at the cut site, peaking at 7.39 ± 1.42% at N/P 8 and decreasing at higher N/P ratios (Figure. 10C). Cell viability remained comparable to the mock sample at lower N/P ratios but decreased significantly at N/P 32 and N/P 64 indicating polymer toxicity at higher N/P ratios (Figure 10D). These results show that P10PSH polyplexes can effectively transfect RNP into HSPC cells, achieving around 6% gene editing with minimal toxicity at optimal N/P ratios.

Revisiting the 2nd generation CRISPR-AuNP, the maximum amount of P10PSH copolymer bound to the particles at 100 pmol dose of RNP was calculated to be equivalent to N/P 0.5 suggesting the 2nd generation CRISPR-AuNP carried insufficient cationic polymer to achieve endosomal escape in HSPC.

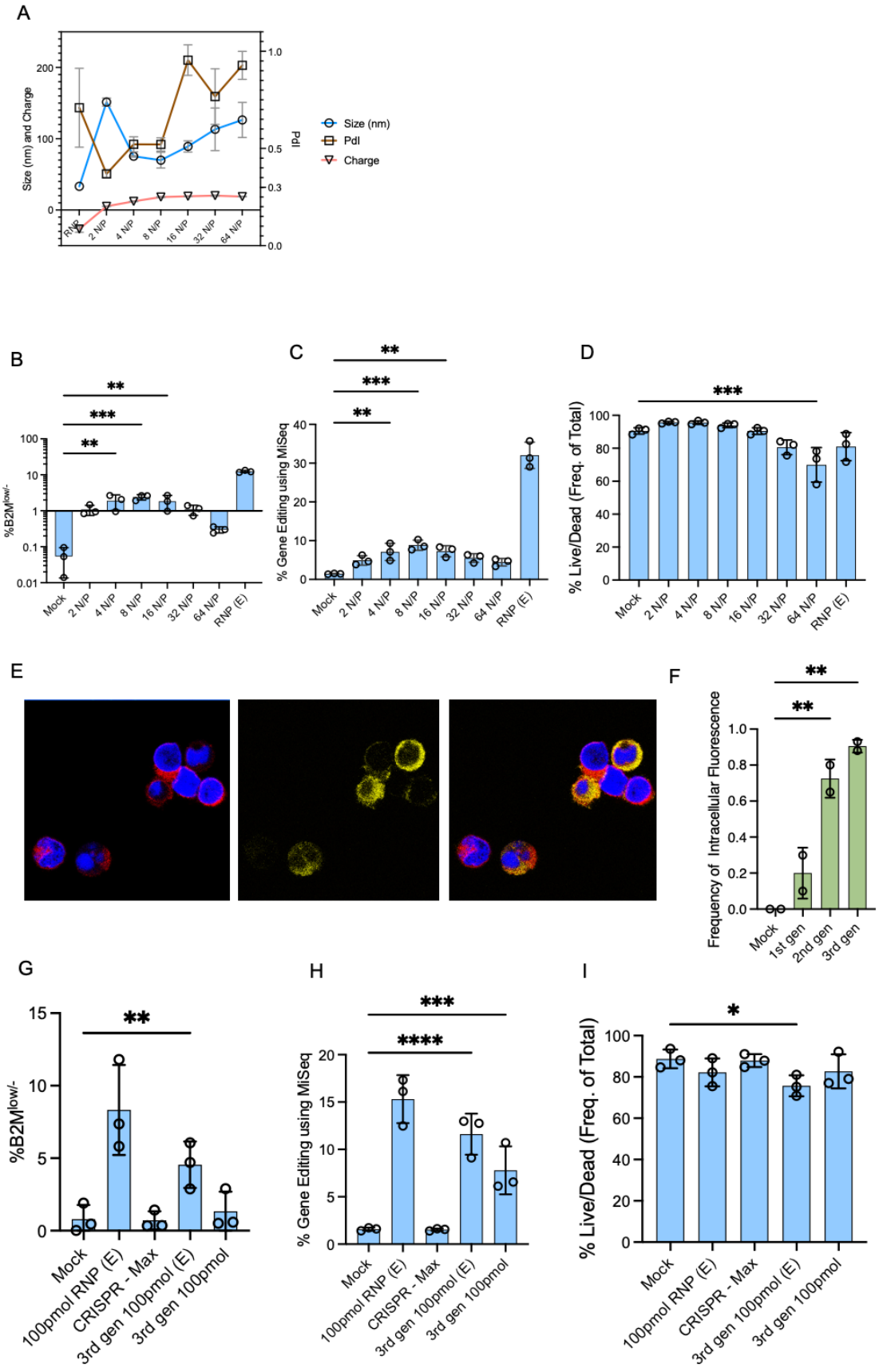
A
Size (nm) and Charge
PdI
Size (nm)
PdI
Charge
RNP
2 N/P
4 N/P
8 N/P
16 N/P
32 N/P
64 N/P
B
%B2M low/-
Mock
RNP (E)
C
% Gene Editing using MiSeq
D
% Live/Dead (Freq. of Total)
E
F
Frequency of Intracellular Fluorescence
Mock
1st gen
2nd gen
3rd gen
G
%B2M low/-
100pmol RNP (E)
CRISPR - Max
3rd gen 100pmol (E)
3rd gen 100pmol
H
% Gene Editing using MiSeq
I
% Live/Dead (Freq. of Total)

Figure. 10 | 3rd generation CRISPR-AuNP display favorable nanoformulation characteristics, endosomal escape and in vitro gene editing in HSPC.

A) DLS analysis of Cas9 RNP polyplexes with P10PSH copolymer at N/P ratios 2–64. Data are means ± SEM (n=3 technical replicates).

B) Percentage of $B2M^{low/-}$ cells in CD34+ HSPCs treated with P10PSH polyplexes (100 pmol RNP) at N/P ratios 2–64, measured by flow cytometry. Data are means ± SEM (n=3 biological replicates).

C) Indel frequency at the B2M gene in CD34+ HSPCs treated with P10PSH polyplexes at N/P ratios 2–64, determined by DNA sequencing. Data are means ± SEM (n=3 biological replicates).

D) Viability of CD34+ HSPCs treated with P10PSH polyplexes at N/P ratios 2–64, assessed by live/dead staining via flow cytometry. Data are means ± SEM (n=3 biological replicates).

E) Confocal microscopy of CD34+ HSPCs treated with 3rd generation CRISPR-AuNP containing ATTO550-labeled tracrRNA (yellow) after 6 hours of incubation. Plasma membrane stained with CellMask Deep Red (red), nucleus with NucBlue (blue). Scale bar, 10 μm.

F) Frequency of trRNA+ signal measured in cells using confocal microscopy

G) Percentage of $B2M^{low/-}$ cells in CD34+ HSPCs treated with 3rd generation CRISPR-AuNP (100 pmol RNP), measured by flow cytometry. Data are means ± SEM (n=3 biological replicates).

H) Indel frequency at the B2M gene in CD34+ HSPCs treated with 3rd generation CRISPR-AuNP (100 pmol RNP), determined by DNA sequencing. Data are means ± SEM (n=3 biological replicates).

I) Viability of CD34+ HSPCs treated with 3rd generation CRISPR-AuNP, assessed by live/dead staining via flow cytometry. Data are means ± SEM (n=3 biological replicates).

Synthesis of a 3rd generation CRISPR-AuNP with intact copolymer equivalent to N/P 8

Since sequentially layering RNP and then copolymer onto AuNP was insufficient to achieve the polymer doses required for endosomal escape in HSPCs, we next explored an all-in-one loading approach. We hypothesized that preforming RNP and P10PSH copolymer at an N/P ratio of 8 before adding AuNP cores could result in a more stable CRISPR-AuNP formulation with sufficient copolymer content for intracellular delivery. We anticipated that P10PSH polyplexes with RNP containing thiolated gRNAs could enable covalent crosslinking via disulfide bridges. Free thiols remaining on the copolymer could then form covalent bonds with the AuNP surface upon interaction, preserving integrity of the cargo.

To synthesize stable, conjugated CRISPR-AuNP polyplexes, we first determined the optimal amount of AuNP required to conjugate 100 pmol of N/P 8 RNP polyplexes. Keeping the RNP polyplex concentration constant at 100 pmol, we incrementally increased the amount of 17nm AuNP added and monitored conjugation efficiency using DLS. The size of CRISPR-AuNP conjugated polyplexes decreased as the AuNP concentration increased, with the

smallest size observed being 103.3 ± 1.62 nm at 20 μg of AuNP (Figure. 11). At this concentration, the zeta potential approached near neutrality (~1 mV), indicating polyplexes were fully conjugated or at least associated with the AuNPs in solution, even in the absence of low pH conditions. CRISPR-AuNP synthesized using this approach were designated as 3rd generation CRISPR-AuNP.

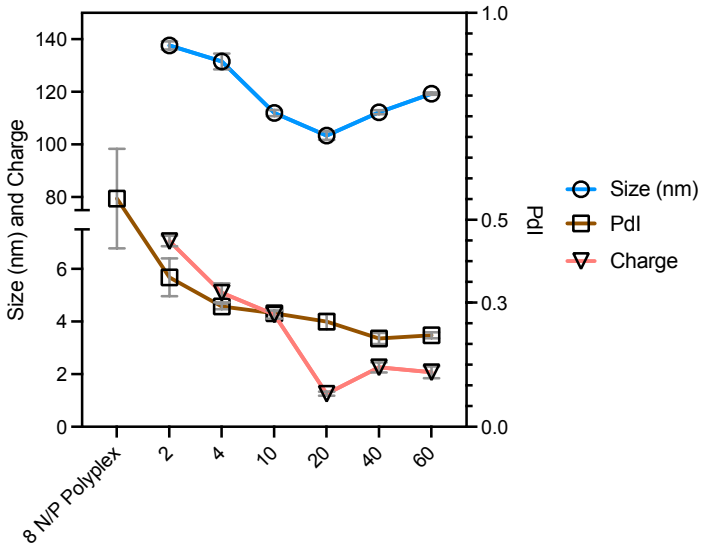

Figure 11 | Optimization of AuNP quantity for 3rd generation CRISPR-AuNP synthesis.

DLS of particles formed by conjugating 100 pmol Cas9 RNP polyplexes (N/P ratio 8, P10PSH) with varying amounts (0–20 μg) of AuNP cores. Particle size decreased with increasing AuNP concentration, reaching 103.3 ± 1.62 nm at 20 μg AuNP. Data are means ± SEM (n=3 technical replicates).

To confirm Cas9 RNP loading onto 3rd generation CRISPR-AuNP, we performed SDS-PAGE analysis as previously described. SDS-PAGE analysis revealed an estimated 39.6 ± 7.7 RNP/AuNP core (Figure. 12). In-tube dsDNA cutting assay demonstrated two distinct bands indicating Cas9 RNP retained activity after conjugation in 3rd generation CRISPR-AuNP (Figure. 13).

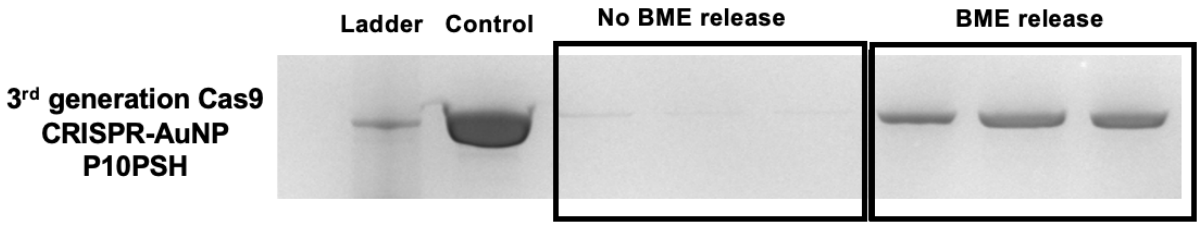

Figure. 12 | 3rd generation CRISPR-AuNPs successfully loads Cas9 protein synthesized with P10PSH polyplexes.

SDS-PAGE analysis of protein released from 3rd generation CRISPR-AuNPs made with P10PSH poylplexes. Distinct bands corresponding to Cas9 protein (~162 kDa) are visible. Visible ladder band is 130 kDa MW.

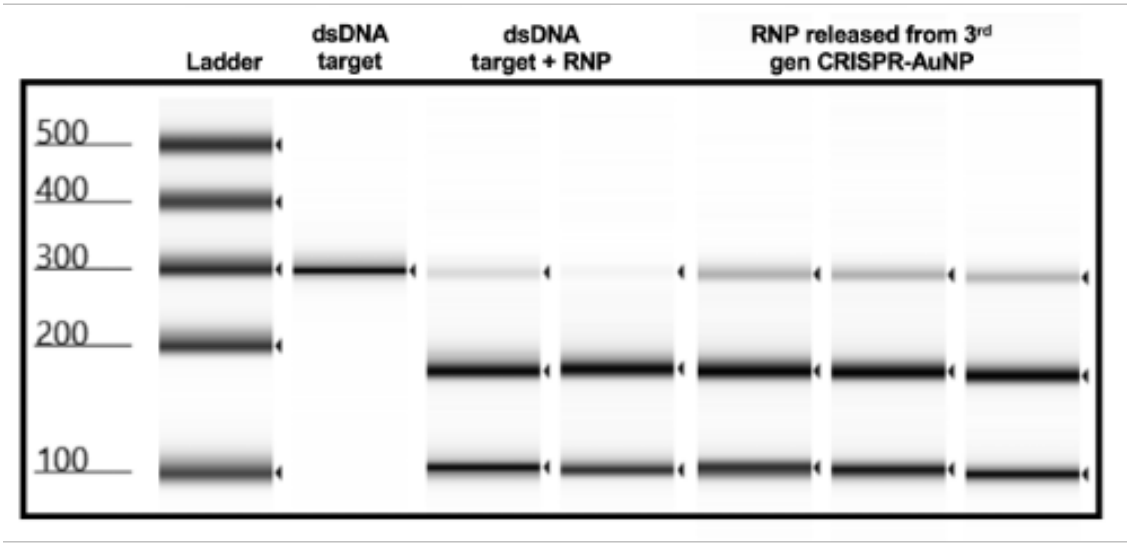

Figure. 13 | Released Cas9 from 3rd generation CRISPR-AuNPs cleaves target DNA.

TapeStation gel images showing DNA cutting assay with Cas9 RNP released from 3rd generation CRISPR-AuNPs. The intact DNA template (upper band) and the cleavage products (lower bands) are visible.

Delivery of gene editing by 3rd generation CRISPR-AuNP in HSPC

We labeled trRNA with ATTO550 to track Cas9 RNP intracellular localization following treatment of HSPC with 3rd generation CRISPR-AuNP. Confocal microscopy revealed ATTO550-conjugated trRNA dispersed throughout the cytoplasm after 6 hours, suggesting successful Cas9 RNP endosomal escape (Figure. 10E), with overall cellular fluorescence more widely distributed compared to 2nd generation CRISPR-AuNP (Figure. 4F).

We treated HSPCs with 3rd generation CRISPR-AuNP containing 100 pmol of RNP and 62 μg of AuNP, as determined by SDS-PAGE. Flow cytometry analysis showed detectable but statistically insignificant B2M knockout (Figure. 10G), with no adverse impact on cell viability. Sequencing and gene editing analysis demonstrated 7.8 ± 2.52% (Figure. 10H) indels at the target site, a statistically significant result ($p < 0.05$), comparable to the 8.83 ± 1.32% gene editing efficiency observed with free polyplex administration at the same dose at 8 N/P (Figure. 10C). Importantly, 3rd generation CRISPR-AuNP exhibited higher gene editing efficiency compared to Lipofectamine™ CRISPRMAX™ at equivalent RNP doses (Figure. 10H). CRISPRMAX™, a commercially available lipid reagent for CRISPR RNP delivery, has demonstrated efficacy in cell lines but limited success in primary cells. These findings confirm

that 3rd generation CRISPR-AuNP internalizes into HSPCs and edits the B2M gene while maintaining cell viability, but higher levels of gene editing are desirable.

Optimizing 3rd generation CRISPR-AuNP to increase gene editing

To further enhance delivery efficiency, we tested the impact of thiol-PEG grafting . We synthesized polyplexes with increasing thiol-PEG grafting using 2k MW PEI functionalized with 2k MW PEG-SH at varying amounts (2% grafted – P02PSH, 6% grafted – P06PSH, 10% grafted – P10PSH, and 20% grafted – P20PSH), and tested gene editing in HSPCs at different N/P ratios. We observed increasing PEG grafting and thiol content on the polymer correlated with higher B2M knockout efficiency (Figure. 14A), particularly at low N/P ratios. At N/P 2, B2M knockout efficiency increased from 0.71 ± 0.42% (P02PSH) to 12.18 ± 5.06% (P20PSH) (Figure. 14B). However, as the N/P ratio increased, a significant drop in cell viability was also observed (Figure 14C).

We formulated 3rd generation CRISPR-AuNP with P20PSH polyplexes by conjugating them to AuNPs using the previously described method, with a slight modification. We first formed polyplexes as before but modified the synthesis by then adding concentrated AuNPs. This approach resulted in CRISPR-AuNP with a hydrodynamic diameter of 49.47 ± 0.34 nm and a PdI of 0.068 ± 0.003, and zeta potential of -15.7 ± 0.15 mV. Polyplexes made with P20PSH at 2 N/P ration demonstrated a hydrodynamic diameter of 46.25 ± 25.62 nm and a PdI of 0.354 ± 0.08, with a zeta potential of -7.15 ± 2.65 mV by DLS (Figure. 14D).

Since the RNP itself is ~17 nm, its theoretical size when conjugated to a 17 nm AuNP core would be ~47 nm (assuming a RNP radius of 15 nm on both sides of the AuNP core). To verify whether a unilayer of RNP and polymer had formed, we performed cryo-transmission electron microscopy (TEM). Imaging confirmed the presence of an RNP layer along with polymer on the AuNP surface, supporting the successful conjugation of polyplexes to AuNPs (Figure. 14E). SDS-PAGE demonstrated bands corresponding to Cas9, with 35 RNP/AuNP core (Figure. 15).

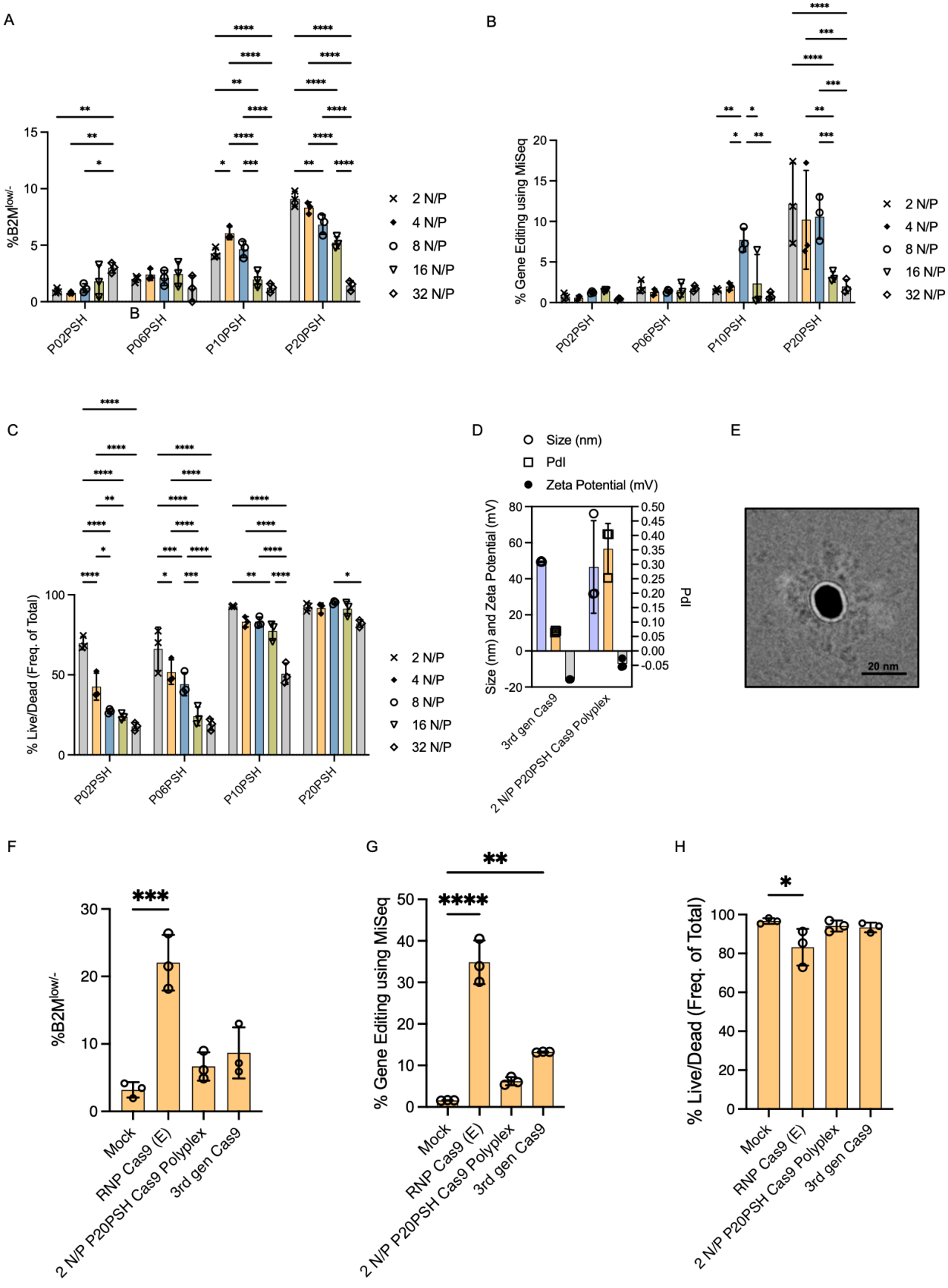
A
%B2M^low/-
2 N/P
4 N/P
8 N/P
16 N/P
32 N/P
P02PSH
P06PSH
P10PSH
P20PSH
B
% Gene Editing using MiSeq
C
% Live/Dead (Freq. of Total)
D
Size (nm)
PdI
Zeta Potential (mV)
Size (nm) and Zeta Potential (mV)
3rd gen Cas9
2 N/P P20PSH Cas9 Polyplex
E
20 nm
F
Mock
RNP Cas9 (E)
G
H

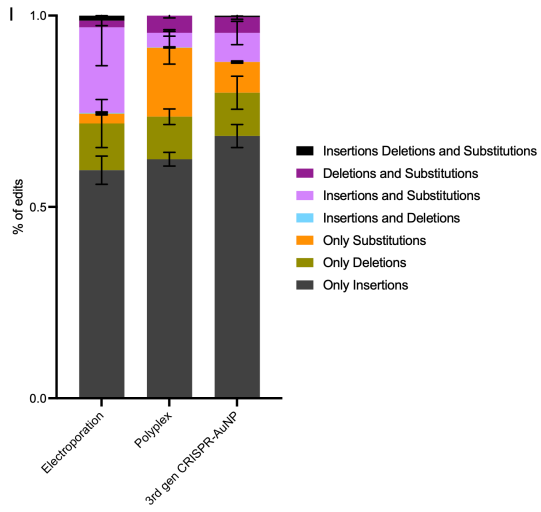

Figure 14 | Increasing PEG-SH grafting enhances gene editing efficiency of 3rd generation CRISPR-AuNP.

A) Percentage of B2M$^{low/-}$ CD34+ HSPCs treated with polyplexes (100 pmol RNP) made with PEI grafted with varying percentages (2%–20%) of PEG-SH (P02PSH–P20PSH) at N/P ratios 2–32, measured by flow cytometry. Data are means ± SEM (n=3 biological replicates).

B) Indel frequency at the B2M gene in CD34+ HSPCs treated with P02PSH–P20PSH polyplexes at N/P 2, determined by DNA sequencing. Data are means ± SEM (n=3 biological replicates).

C) Viability of CD34+ HSPCs treated with P02PSH–P20PSH polyplexes at N/P ratios 2–32, assessed by live/dead staining via flow cytometry. Data are means ± SEM (n=3 biological replicates).

D) DLS characterization comparing 3rd generation CRISPR-AuNP (P20PSH, 2 N/P) and P20PSH polyplexes alone, showing hydrodynamic diameters and zeta potentials. Data are means ± SEM (n=3 technical replicates).

E) Cryo-TEM image of 3rd generation CRISPR-AuNP (P20PSH, 2 N/P) showing AuNP core with surrounding RNP and polymer layer. Scale bar, 20 nm.

F) Percentage of $B2M^{low/-}$ CD34+ HSPCs treated with 3rd generation CRISPR-AuNP (P20PSH, 2 N/P) versus P20PSH polyplexes alone (100 pmol RNP), measured by flow cytometry. Data are means ± SEM (n=3 biological replicates).

G) Indel frequency at the B2M gene in CD34+ HSPCs treated with optimized 3rd generation CRISPR-AuNP (P20PSH, 2 N/P) versus P20PSH polyplexes, determined by DNA sequencing. Data are means ± SEM (n=3 biological replicates).

H) Viability of CD34+ HSPCs treated with optimized 3rd generation CRISPR-AuNP (P20PSH, 2 N/P), assessed by live/dead staining via flow cytometry. Data are means ± SEM (n=3 biological replicates).

I) Type of indels at B2M locus when RNP delivered via Electroporation, Polyplex and 3rd generation CRISPR-AuNP. Data are means ± SEM (n=3 biological replicates).

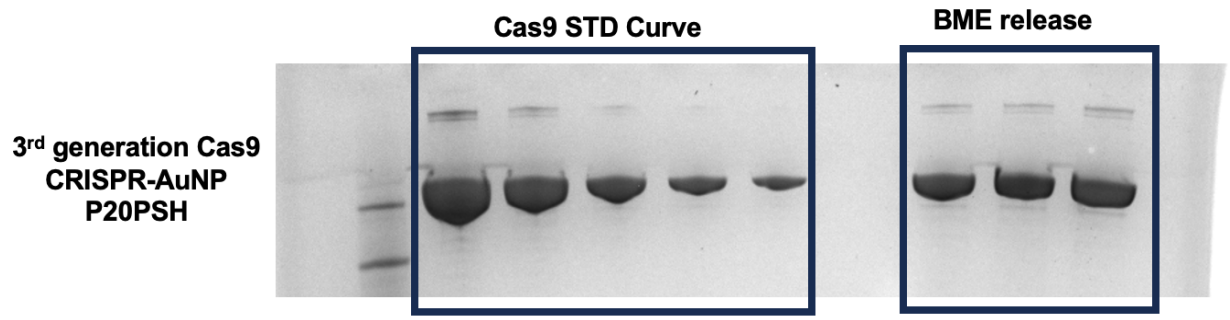

Figure. 15 | 3rd generation CRISPR-AuNPs successfully loads Cas9 protein synthesized with P20PSH polyplexes

SDS-PAGE analysis of protein released from 3rd generation CRISPR-AuNPs made with P20PSH. Left lanes show Cas9 standards (100, 50, 25, 12.5, 6.25 pmol). Distinct Cas9 bands (~162 kDa) visible in BME release lanes. Top ladder band is 130 kDa MW.

Enhanced activity of 3rd generation CRISPR-AuNP in HSPC

We prepared polyplexes at a 2 N/P ratio using P20PSH and 100 pmol of RNP, as well as 3rd generation CRISPR-AuNP at the same cargo doses and treated HSPC. After 72 hours, we observed 8.6 ± 3.78% $B2M^{low/-}$ cells treated with 3rd generation CRISPR-AuNP whereas only 6.6 ± 2.1% of HSPC treated with 2 N/P P20PSH polyplexes were $B2M^{low/-}$(Figure. 14F). Sequencing and gene editing analysis followed a similar trend, with an indel frequency of 13.23 ± 0.12% in cells treated with 3rd generation CRISPR-AuNP, and 6.19 ± 0.97% in cells treated with 2 N/P P20PSH polyplexes (Figure. 14G). These results suggest that the presence of AuNP cores effectively doubled the gene editing efficiency observed with polyplexes alone at the same RNP dose in HSPC cells and achieved a total editing >10%. Modifications to the 3rd generation synthesis implemented for addition on P20PSH also reduced the total amount of

nuclease protein required for assembly. Research-grade 3rd generation CRISPR-AuNP consisting of Cas9 costs $64 per 1x10^6 HSPC treated, with >90% of cost attributed to nuclease protein (Table. 1).

Table 1: Cost of components to synthesize 100 pmols of CRISPR-AuNP sufficient to treat 500,000 cells

Components	100 pmols of CRISPR-AuNP*
Nuclease	$31.52
Modified crRNA	$0.074
tracrRNA	$0.57
AuNP Cores	$0.0062
Polymer	$0.036

*dose relative to pmol of RNP.

3rd Generation CRISPR-AuNP Assembly with Alternative CRISPR Systems

We next tested 3rd generation CRISPR-AuNP assembly with Cas12a and MG29-1, two alternative CRISPR systems. Cas12a is a class 2 type V CRISPR system that consists of a single crRNA and recognizes T-rich PAM sequences (TTTV, where V is A, C, or G).[99] The result of Cas12a activity is a double-stranded DNA break with a 5bp overhang, in contrast to Cas9's blunt-end cuts. MG29-1 is a more recently discovered type V CRISPR nuclease that recognizes an AT-rich PAM sequence and produces a staggered cut[100]. For each, optimal gRNA targeting

the B2M gene were synthesized with the same 12-unit OEG spacer and terminal thiol, however, the end modified differed for each gRNA (Table 2). For each, we used the 100 pmol dose of RNP to assemble 3rd generation CRISPR-AuNP with P20PSH co-polymer as described above for Cas9. DLS for Cas12a-containing particles indicated a hydrodynamic diameter of 77.5 ±1.77 nm, PdI of 0.14 ± 0.05, and zeta potential of -12.73 ± 1.5 mV (Figure. 17A). For MG29-1, DLS showed particles with a hydrodynamic diameter of 46.89 ± 1.19 nm, PdI of 0.089 ± 0.00, and zeta potential of -12.06 ± 1.69 mV (Figure. 17A). SDS-PAGE confirmed 40 Cas12a RNP/AuNP and 39 MG29-1 RNP/AuNP, respectively (Figure. 16). Treatment of primary human HSPC resulted in no observable toxicity for either nuclease. For Ca12a, we do not expect protein knockdown as the gRNA targets a intronic B2M region, but we observe d8.64 ± 1.07 % $B2M^{low/-}$ cells for MG29-1 3rd generation CRISPR-AuNP treated HSPC (Figure. 17B). For Cas12a and MG29-1, respectively, corresponding levels of indels were 15.07 ± 1.9% and 13.39 ± 1.5%. (Figure. 17C, 17E). For Cas12a, 3rd generation CRISPR-AuNP outperformed polyplexes alone, as observed for Cas9, but we observed no difference between editing levels achieved for MG29-1 polyplexes when compared to 3rd generation MG29-1 CRISPR-AuNP.

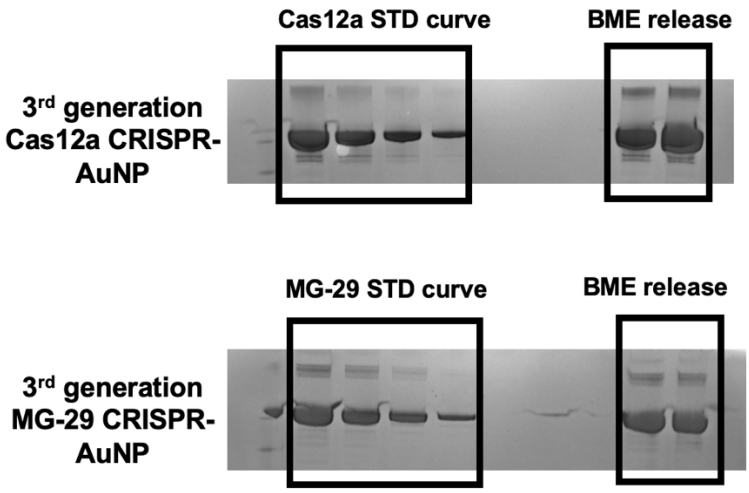

Figure. 16 | 3rd generation CRISPR-AuNPs successfully loads Cas12a and MG-29 protein synthesized with P20PSH polyplexes

SDS-PAGE analysis of protein released from 3rd generation CRISPR-AuNPs made with P20PSH. Left lanes show standard curve (50, 25, 12.5, 6.25 pmol). Distinct Cas12a bands and MG-29 bands visible in BME release lanes. Top ladder band is 130 kDa MW.

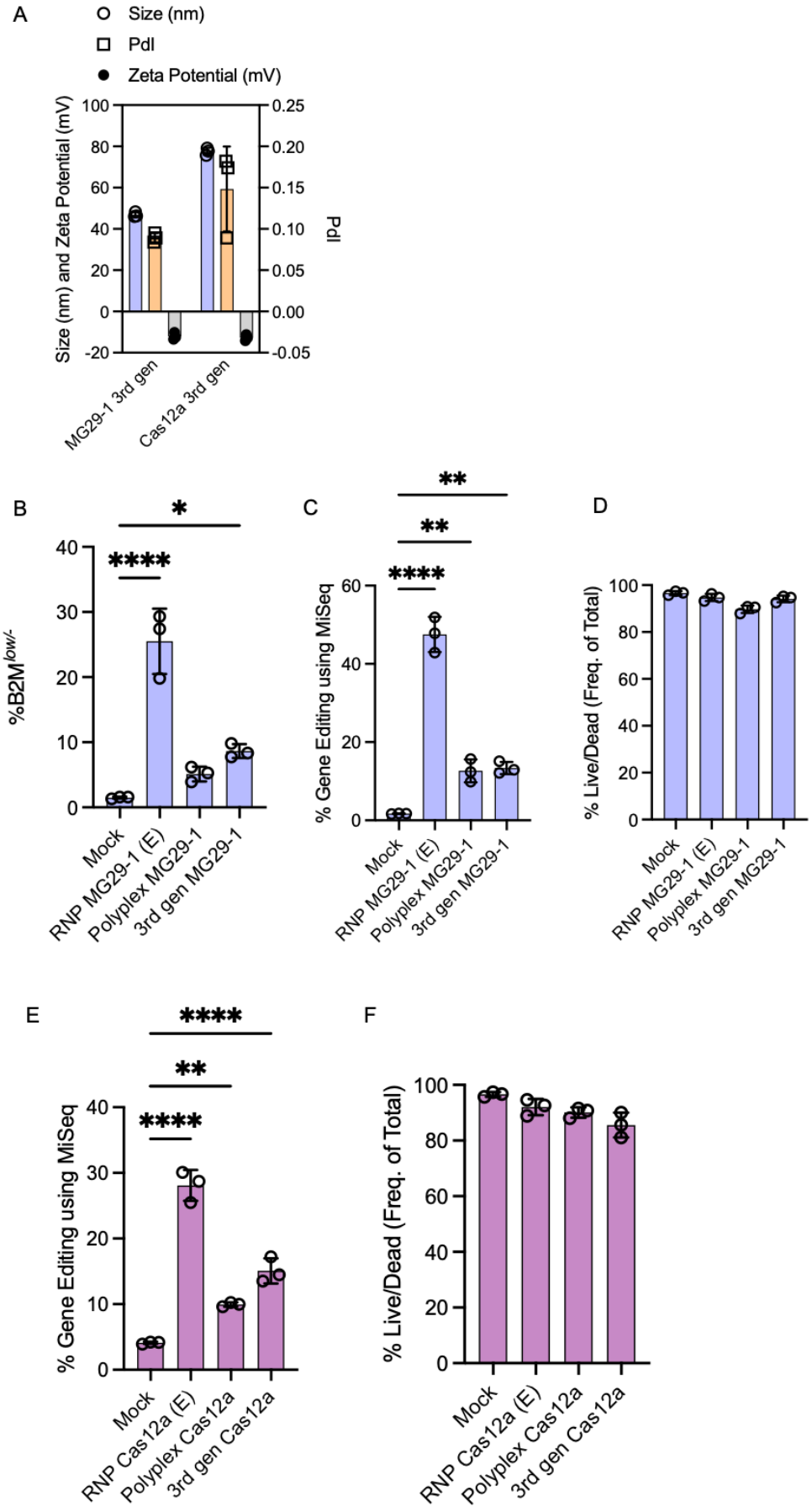
A
Size (nm)
PdI
Zeta Potential (mV)
Size (nm) and Zeta Potential (mV)
PdI
MG29-1 3rd gen
Cas12a 3rd gen
B
%B2M low/-
Mock
RNP MG29-1 (E)
Polyplex MG29-1
3rd gen MG29-1
C
% Gene Editing using MiSeq
D
% Live/Dead (Freq. of Total)
E
% Gene Editing using MiSeq
RNP Cas12a (E)
Polyplex Cas12a
3rd gen Cas12a
F
% Live/Dead (Freq. of Total)

Figure 17 | 3rd generation CRISPR-AuNP platform delivers multiple CRISPR nucleases to HSPCs.

A) DLS characterization of 3rd generation CRISPR-AuNP formulated with Cas12a and MG29-1 nucleases, showing hydrodynamic diameter and zeta potential measurements. Data are means ± SEM (n=3 technical replicates).

B) Percentage of $B2M^{low/-}$ CD34+ HSPCs treated with MG29-1 3rd generation CRISPR-AuNP (100 pmol RNP), measured by flow cytometry. Data are means ± SEM (n=3 biological replicates).

C) Indel frequency at the B2M gene in CD34+ HSPCs treated with MG29-1 3rd generation CRISPR-AuNP, determined by DNA sequencing. Data are means ± SEM (n=3 biological replicates).

D) Viability of CD34+ HSPCs treated with MG29-1 3rd generation CRISPR-AuNP, assessed by live/dead staining via flow cytometry. Data are means ± SEM (n=3 biological replicates).

E) Indel frequency at the B2M gene in CD34+ HSPCs treated with Cas12a 3rd generation CRISPR-AuNP, determined by DNA sequencing. Data are means ± SEM (n=3 biological replicates).

F) Viability of CD34+ HSPCs treated with Cas12a 3rd generation CRISPR-AuNP, assessed by live/dead staining via flow cytometry. Data are means ± SEM (n=3 biological replicates).

Discussion

There is high demand for a cost-effective synthetic nanoparticle capable of delivering CRISPR cargo into living primary human cells. The goal of this study was to advance the development of a modular CRISPR-AuNP that can be assembled in a day or less with commercially available materials, requiring no advanced engineering[101]. Our investigation of the previously described 1st generation CRISPR-AuNP revealed instability in the gRNA complex during cargo loading, resulting in loss of active Cas9 RNP on the AuNP surface. To address this, we demonstrated that pre-forming RNP complexes prior to AuNP loading stabilizes the Cas9 RNP, enabling it to withstand loading conditions and form functional RNP monolayers. While this restored particle integrity and CRISPR activity, it initially compromised polymeric coating and reduced endosomal escape in primary HSPCs. Further optimization of cationic polymers improved endosomal escape, and by targeting the human B2M gene, we assessed gene editing efficiency across multiple nanoformulations. Our findings show that the optimized 3rd generation CRISPR-AuNP significantly enhances Cas9 delivery and gene editing efficiency in primary human HSPCs, achieving >10% indels with no observable drop in cell viability, providing a promising non-viral CRISPR delivery strategy for these challenging-to-edit cells. This design was also successfully adapted to Cas12a and MG29-1 with similar ease of assembly yielding >10% editing in HSPCs.

Compared to current clinical electroporation methods, which achieve >40% gene editing in HSPCs at 100 pmol RNP doses but require specialized equipment, buffers, and multi-day processing, our 3rd generation CRISPR-AuNP offers a simpler alternative. In our study,

electroporation of 100 pmol free Cas9 RNP resulted in 47.8 ± 15.3% editing at the B2M gene, with no consistent drops in cell viability across donors, while the 3rd generation Cas9 CRISPR-AuNP achieved 13.23 ± 0.12% editing at the same dose. Although our particle does not yet match electroporation's editing efficiency, it requires no specialized conditions, treatment involves simply adding the particles to cells in culture and cell entry occurs within 6 hours, as confirmed by confocal microscopy. This simplicity reduces processing complexity, but the lower editing efficiency highlights significant room for improvement to reach therapeutic thresholds.

In the broader field, our approach can be contextualized against other non-viral CRISPR delivery systems[32]. Lipid nanoparticles (LNPs), widely explored due to their success in mRNA delivery, typically deliver CRISPR as mRNA or plasmids, relying on HSPC translation. Recent LNP formulations and cell penetrating peptide based RNP delivery have shown promise, with editing efficiencies in cell lines approaching 30–40%, but their performance in primary HSPCs remains less consistent, often requiring higher doses and exhibiting variable toxicity[81]. For example, cell penetrating peptide modified RNP achieved gene editing in HSPC at doses equivalent to 200 pmol RNP, and with observed toxicity [81]. Our CRISPR-AuNP, delivering pre-formed RNP, bypasses translation and, at 100 pmol doses, shows no toxicity, though its ~13% editing efficiency lags behind the optimized LNPs in more permissive cell types.

The modular design of the 3rd generation CRISPR-AuNP also supports its adaptability to alternative CRISPR systems. Our results with Cas12a (15.07 ± 1.9% indels) and MG29-1

(13.39 ± 1.5% indels) show that the platform can accommodate nucleases with distinct gRNA requirements and physicochemical properties, maintaining activity post-assembly. This versatility suggests potential for integrating next-generation tools like prime editors or base editors. Compared to LNPs or viral-like particles, which often necessitate nuclease-specific engineering for RNP loading[101], our approach uses a universal thiol-based conjugation strategy, simplifying adaptation across systems.

While the 3rd generation CRISPR-AuNP shows preferential editing in HSPCs in vitro, it further can be optimized by leveraging active targeting (e.g., antibody conjugation to exploit HSPC endocytosis) to enhance specificity and efficiency. By addressing intracellular delivery barriers and simplifying assembly to a few hours with reagents costing <$70 per million cells treated, this work lays a foundation for accessible CRISPR research tools.

Methods

Materials

All nucleic acids were purchased through IDT (Coralville, Iowa, US). NLS-SpCas9-NLS and NLS-AsCas12a-NLS were purchased from Aldevron (Fargo, North Dakota, US). NLS-MG29-1-NLS was provided by Metagenomi, Inc. (Emeryville, California, US). The chemicals chloroauric acid, sodium citrate dibasic trihydrate, >37% hydrochloric acid, 50% branched 2k PEI, and β-mercaptoethanol (BME) were purchased from Sigma-Aldrich (St. Louis, Missouri, US). For electroporations, the Neon™ Electroporation System 10-µL Kit (Invitrogen, Waltham, MA, USA) was used on the Neon Transfection System (Invitrogen).

Electroporation kit V and Electroporation kits for Primary T-Cell/HSPC were purchased from Lonza (Basel, Switzerland) and used on the Lonza Nucleofector 2b system. All oligonucleotides were purchased from Integrated DNA Technologies (Coralville, Iowa, USA). All antibodies were purchased from Biolegend (San Diego, California, US). Other materials not listed were purchased through Thermo-Fischer Scientific (Waltham, Massachusetts, US).

AuNP core synthesis

Spherical Au nanocores were generated via Turkevich's method[102]. Briefly, chloroauric acid solution (0.25 mM) was brought to its boiling point and then reduced with 3.33% sodium citrate solution under rapid mixing for 15 min. After the solution developed a ruby color, batches were removed from heat and allowed to reach room temperature overnight. The hard diameter of Au cores was determined by transmission electron microscopy (TEM; Talos L120C, ThermoFisher Scientific). Concentration was determined with 1 cm Beer–Lambert law absorbance at 520 nm (Nanodrop One, Thermo-Fischer) with published AuNP core extinction coefficients. Batches of Au cores were then stored at 4°C without further refinement.

1st generation CRISPR-AuNP Synthesis

CRISPR/AuNP were generated according to the method published by Shahbazi et. Al. Au cores were added to an acid-treated 2mL microcentrifuge tube (Corning, Corning, NY, USA). All incubation steps were carried out at room temperature on the benchtop. All washes utilized

an Eppendorf 5702 RH centrifuge at 15 krcf, 15 min at 4°C (Eppendorf, Hamburg, Germany). duRNA was generated through equimolar annealing of trRNA/crRNA in duplex buffer (IDT), [duRNA]f = 50 μM. This duRNA was then added via rapid pipetting to Au cores at 2:1 duplex/Au core mass ratio and mixed well. Citrate buffer (500 mM, pH 3.0) was added to 25 mM and the mixture incubated for 30 min at room temperature. Samples were washed with UltraPure Water (UPW; Invitrogen, USA) twice to generate the product designated "AuNP/gRNA" stage. A 1.2 μM solution of Cas9 nuclease protein in UPW was generated in a second acid-treated vial to which AuNP/gRNA was added and incubated for 10 min, yielding the product designated "AuNP/gRNA" stage. 0.1% PEI solution (in UPW, pH 7.0) was added at a 2:1 PEI:Au core mass ratio and quickly mixed via trituration and vortexing before incubating for 10 min and designated "CRISPR-AuNP". Particles were stored at 4 °C.

2nd Generation CRISPR-AuNP Synthesis

2nd Generation CRISPR-AuNP were synthesized by first preforming Cas9 RNP. For Cas9 an equimolar solution of crRNA/trRNA was made in duplex buffer as above, then 2.5:1 duRNA:Cas9 molar solution was made in Dulbecco's phosphate buffered saline (DPBS; Gibco) to a final RNP concentration of 9.2 μM. These RNP solutions were incubated overnight at 4 °C before adding to Au cores at various Au core/RNP mass ratios as described. The solution was incubated on a shaker for 1 hr at room temperature. A 500 mM, pH 3.8 citrate solution was added to the AuRNP solution to a final concentration of 25 μM. This solution was incubated for 5 min before being washed at 5 krcf for 45 min at 4 °C. The product was resuspended into pH 7.4, 10 mM HEPES buffer and designated "AuRNP" stage. A

solution of branched PEI 2k MW-g 10%- PEG 2kSH (PPSH; Nanosoft Polymers, Winston Salem, NC, USA) was made to 1 mg/mL in HEPES buffer, added to AuRNP before incubating over 15 min. Particles were stored at 4°C.

3rd generation CRISPR-AuNP Synthesis

3rd generation CRISPR-AuNP was synthesized by first preforming the Cas9 RNP. 1:1 crRNA to trRNA was prepared in duplex buffer to form the gRNA. Equimolar ratio of gRNA to Cas9 was then incubated in 5 uL PBS for formation of Cas9 RNP. For P10PSH polymer, 200 pmol of RNP was mixed with 40 ug of PEI 2k MW-g 10%- PEG 2kSH polymer stock made in PBS and incubated at room temperature for 1 hour. After polyplex formation, 20 μg of AuNP cores were added to the polyplex in protein lo bind tube. For P20PSH polymer, 100 pmol of RNP was mixed with 10 ug of PEI 2k MW-g 20%- PEG 2kSH polymer stock made in PBS and incubated at room temperature for 1 hour. After polyplex formation, 35 ug of concentrated AuNP cores in 30 uL volume were added to the polyplexes and incubated at RT for 1 hour. After 1 hour incubation, the tube was volumed up to 2 mL using UPW and centrifuged at 5000 rcf at 4 C for 1 hour. The supernatant was discarded and the AuNP pellet was resuspended in 50 uL PBS.

DLS and TEM

Particle size and zeta potential were quantified with a Malvern Zetasizer Nano-ZS (Malvern, Worcestershire, UK) at 10 μg/mL in formulation buffer (UPW/HEPES) for DLS, or 10 mM

HEPES for zeta potential. DLS readings were three averaged runs of 10 sub runs at 25 °C in BRAND 40 µL disposable cuvettes (BrandTech Scientific, USA). Zeta potential measurements were averaged over 3 reads at 20°C using autosense for each read in bent capillary cells (Malvern). Particle TEM was run on Talos L120C using 1% uranyl acetate as the negative stain. AuNP core diameter was quantified by drawing a vertical and horizontal cross over each particle and averaging these measurements (n = >10 particles).

DNA Cutting Assay

DNA cutting assays were performed following New England Biolabs (NEB) method[39,40]. Briefly, genomic DNA was extracted from primary isolated HSPC cells (STEMCELL Technologies, Vancouver, BC, Canada) using a PureLink® Genomic DNA Minikit (Invitrogen). The target amplicon DNA containing the desired CRISPR cut site was extracted using primers (Table 2), amplified with Q5® Hot Start 2x Master Mix (New England Biolabs, Ipswich, Massachusetts, US). Target DNA was purified with a PureLink® PCR cleanup kit (Invitrogen). 500 ng of target DNA was then added to PCR strip tubes, along with 1x NEB 3.1r buffer (New England Biolabs). Cas9 preformed RNP was a positive control and AuNP samples at various stages were added at 5 ug Au core ± BME (Sigma-Aldrich), Vt = 50 µL. For CRISPR-AuNP at polymer stage, heparin was added to the reaction for PEI to bind to heparin and not interfere with the cutting assay. Resulting Samples were vortexed before incubation at 37 °C for 15 min. Samples then had 1 µL Proteinase K and 1 µL RNase A added (both from Invitrogen) and were incubated for 10 min at 28 °C, then 10 min at 32 °C before

being heated to 95 °C to denature and cooled to 23 °C over 15 min. DNA samples were resolved for size on TapeStation (Agilent, Santa Clara, California, US) for quantification.

Fluorescent tr/crRNA Loading Quantification

The level of cr/trRNA binding were simultaneously determined by generating 1st generation AuRNA using crRNA-ATTO488 and trRNA-ATTO550. For all RNA-only controls, AuNP core storage solution was used after removing the AuNP cores at 21 krcf for 10 min at 4 °C to mimic synthesis conditions. Following each centrifugation step supernatant was reserved. The final AuNP/gRNA samples had bound RNA released by BME at 100 μM with overnight incubation at 4 °C. After BME release, Au cores were spun out at 21 krcf, 10 min at 4 °C to remove interference. Supernatants were then diluted into pH 7.4 DPBS and all trRNA-ATTO550 and crRNA-ATTO488 in the supernatant quantified using the Spark 10M plate reader.

SDS-PAGE Cas Nuclease Binding Determination

CRISPR-AuNP were synthesized as previously described. After synthesis, the formulation was pelleted (5 krcf, 45 minutes, 4°C) and supernatant removed. Particles were then resuspended in 5 mM BME in DPBS for overnight incubation at 4°C to release RNP from the AuNP core. AuNP cores were removed from the supernatant by centrifugation, then SDS-PAGE was performed using NuPAGE™ 4-12% Bis-Tris Mini Protein Gels (Invitrogen) according to the manufacturer's protocol. Gels were stained with SimplyBlue SafeStain (LC6060) using the

manufacturer's protocol and imaged using an Invitrogen iBright Imaging System. Band intensity was quantified using ImageJ software (version: 1.51j8) and compared to a standard curve generated with known amounts of Cas9 nuclease.

Cas9 pH Stability Quantification

Preformed Cas9 RNP was prepared in Protein LoBind tubes (Eppendorf) according to the 2nd generation CRISPR-AuNP synthesis protocol. 500 μL of AuNP cores (45 mg/mL) and 6.7 μL (100pmol) of Cas9 RNP were mixed in Protein LoBind tubes and placed on a table shaker at low-medium speed for 1 hour at room temperature. 500 mM citrate buffer was formulated in 2 mL Eppendorf tubes by adding citrate to UPW and HCl (>37%) to achieve the final pH of 2.5-4 for Cas9. Citrate was combined to 25 mM with AuNP solution and samples were incubated for 15 minutes at room temperature. Samples were spun at 5 krcf for 45 minutes at 4 °C, and supernatant was removed. Pellets were resuspended in 100 μL of 5 mM BME in 1x DPBS, then incubated on an orbital shaker at 300 rpm for 1 hour at 37 °C. AuNP cores were then removed by centrifugation at 5 krcf for 15 minutes at 4 °C. 70 μL of supernatant was collected in Protein LoBind tubes for DNA cutting assay as described above.

β-2 microglobulin gRNA Optimization

All possible B2M exonic gRNA were identified using Benchling [Biology Software] (Version: 2023-24, San Francisco, California, USA). From these guides, 20 were selected using combined Lindel Cas9 prediction[93] and homology directed repair likelihood based on Tatiossian et al[103].

An additional 6 gRNA were pulled from the promoter region which Lindel did not identify. Jurkat cells (E6-1, ATCC, Manassas, Virginia, USA) were cultured in Gibco Roswell Park Memorial Institute (RPMI)-1640 media + 10% heat inactived fetal bovine serum (FBS) + 1% Penicillin/Streptomycin (ThermoFisher) at 5% CO_2, 37 °C, normoxic conditions for 2 passages before use. crRNA was acquired from IDT and Jurkat cells were electroporated according to Neon Transfection manufacturers protocol for Jurkat Cells. Cells were cultured for 3 days, then analyzed by flow cytometry for cell surface B2M protein expression with phycoerythrin (PE)-conjugated anti-human B2M antibody, clone 2M2 (Biolegend). Flow cytometry was performed on a FACSCelesta (BD Life Sciences, Franklin Lakes, NJ, USA) and data were analyzed using FlowJo™ v 10.9 Software (BD Life Sciences). For DNA sequencing, gDNA was extracted using full B2M gene primers (Table 2) and amplified with Q5® Hot Start 2x Master Mix (New England Biolabs, Ipswich, Massachusetts, US). The target DNA was purified by PureLink® PCR cleanup (Invitrogen), then the target exon was extracted with B2M exon primers with attached Nextera XT DNA Library Preparation Kit (Illumina, San Diego, Ca, USA) index adapter sequences. The PCR amplicons were cleaned up and unique indexes attached to the samples before being run on a MiSeq v2 chip (Illumina), read depth >10000 per sample. Genetic editing analysis was completed using r CRISPRESSO bioinformatics tool.

HSPC Cell Culture

Primary human HSPCs were sourced from the Core Center of Excellence in Hematology at the Fred Hutchinson Cancer Center following mobilization of healthy adult donors with G-

CSF (Amgen, Thousand Oaks, CA, USA), under a protocol approved by the Fred Hutch Institutional Review Board (protocol no. 985.03) and compliant with the Declaration of Helsinki and Belmont Report. Cells were cultured in StemSpan™ Serum-Free Expansion Medium version II (SFEM II; STEMCELL Technologies) supplemented with 50 ng/mL each of recombinant human stem cell factor (SCF; Peprotech, Cranbury, NJ, USA), thrombopoietin (TPO; CellGenix, Freiburg, Germany), and Flt-3 ligand (CellGenix, Freiburg, Germany). Following thaw, HSPCs were resuspended in pre-warmed medium and subjected to an overnight pre-treatment incubation at 37°C with 5% CO2 under normoxic conditions before further experimental use.

CRISPR-AuNP and Polyplexes Treatment of Cells

Primary human HSPCs were thawed from cryopreservation into SFEM II and supplemented with growth factors - Stem Cell Factor (SCF), Fms-like tyrosine kinase 3 ligand (Flt-3 ligand) and Thrombopoietin (TPO) before being pre-stimulated overnight at 37°C in a humidified 5% CO2 incubator. After overnight incubation, the cells were washed twice with DPBS at 1500 rpm for 8 min and were resuspended in plain IMDM (Gibco Iscove's Modified Dulbecco's Medium). A total of 500,000 cells were then seeded in 150 mL of IMDM media in a 96 well plate. After 2 hours of incubation in serum-free IMDM media, CRISPR-AuNP formulation was added and was incubated for 5 hours. After 5 hours, the cells were transferred to 48 well plate and 800 uL of SFEM II supplemented media was added. For CRISPR-Max (Lipofectamine™ CRISPRMAX™ Thermofisher), the manufacturer's protocol was used. All

treatments were performed in triplicate against three independent human cell donors (biological replicates). After 72 hours of incubation at 37°C in a humidified 5% CO_2 incubator, cells were washed with DPBS and harvested for flow cytometry and genomic DNA (gDNA) extraction for gene editing analysis. Polyplex treatment was conducted under identical conditions to the CRISPR-AuNP treatment, with varying polymer quantities (N/P ratios) mixed with ribonucleoprotein (RNP) complexes and applied to cells.

Electroporation of CRISPR-AuRNP

CRISPR-AuNP generations were synthesized to the RNP-AuNP stage. Nanoformulations were washed twice in 10 mM HEPES for 2nd generation CRISPR-AuNP buffer at 5 krcf for 45 min at 4°C, then resuspended in 50 μL of 10 mM HEPES/DPBS buffer and electroporated into cells using a Neon transfection system with 100 μL electroporation tips. The electroporation parameters for transfection of HSPC included an electrical potential of 1600 V, pulse width of 10 msec over three pulses.

PCR conditions for B2M amplifications and MiSeq Sequencing

PCR amplification of the B2M gene was performed using Q5 Hot Start High-Fidelity 2X Master Mix (New England Biolabs) in a final reaction volume of 50 μL. The reaction mixture comprised 25 μL of 2X master mix, 10 μM each of forward and reverse primers, 10 ng genomic DNA, and nuclease-free water. The Q5 master mix was selected for its high fidelity and specificity. Thermal cycling was conducted on a thermal cycler (Eppendorf Mastercycler

x50s) under the following conditions: an initial denaturation at 98°C for 30s, followed by 30 cycles of denaturation at 98°C for 10s, annealing at 65°C for 20s, and extension at 72°C for 30s. A final extension step was performed at 72°C for 5 min, and samples were held at 4°C. MiSeq was performed on the amplicons based on manufacturers (Illumina) protocol using Nextera Indexes.

Confocal Microscopy

G-CSF mobilized HSPCs from three independent donors were thawed and plated in SFEM II media supplemented with 50 ng/mL TPO, Flt-3 ligand, and SCF. Cells were incubated overnight as described above before treatment and were treated with CRISPR- AuNP with conditions described above. CRISPR-AuNP were synthesized as previously described with a fluorescently labeled ATTO550 trRNA. 6 hours after nanoparticle addition, cells were washed in DPBS twice before staining with NucBlue Live Cell Stain (Hoechst 33342, ThermoFisher) and CellMask Deep Red membrane stain (ThermoFisher) according to manufacturer's protocol. Cells were washed twice more in DPBS and resuspended in DPBS with 2% FBS for acquisition on a Zeiss LSM 780 confocal microscope (Oberkochen, Germany). Images were acquired using a 63x oil immersion objective at 0.8x zoom for widefield capture.

Statistical analysis

Graphpad Prism (10.0.4; Boston, Ma, USA) was used to present all results as the mean ± SEM. Two group comparisons used Student's t-test. Multiple group comparisons used Tukey posthoc test and one-way ANOVA. The threshold for statistical significance was $\alpha < 0.05$.

Table 2: Primers and gRNA sequences

Name	Sequence
B2M_FullGene_FP	CTAACCTGGCACTGCGTCG
B2M_FullGene_RP	GTCTGCATACTCCTCATGACCTG
B2M_Exon1_FP	TCGTCGGCAGCGTCAGATGTGTATAAGAGACAGTAACCTGGCACTGCGTC
B2M_Exon1_RP	GTCTCGTGGGCTCGGAGATGTGTATAAGAGACAGCCAAAGGTCTCCCCTGC
B2M_Exon2_FP	TCGTCGGCAGCGTCAGATGTGTATAAGAGACAGGACACCAAGTTAGCCCCAA
B2M_Exon2_RP	GTCTCGTGGGCTCGGAGATGTGTATAAGAGACAGCATTCAGGGTAGTATGGCCATAG
B2M_Exon3_FP	TCGTCGGCAGCGTCAGATGTGTATAAGAGACAGGGAACAGCAGCCTATTCTGC
B2M_Exon3_RP	GTCTCGTGGGCTCGGAGATGTGTATAAGAGACAGCAGGTAATGTGGGTAACCACC
B2M_Exon4-1_FP	TCGTCGGCAGCGTCAGATGTGTATAAGAGACAGGACAAGTTTGGTAATGAGATCTGC

B2M_Exon4-1_RP	GTCTCGTGGGCTCGGAGATGTGTATAAGAGACAGGCAAGAGATTGAAGAGTTCAAATCTG
B2M_Exon4-2_FP	TCGTCGGCAGCGTCAGATGTGTATAAGAGACAGCTCAAAGCTTGTTAAGATAGTTAAGCG
B2M_Exon4-2_RP	GTCTCGTGGGCTCGGAGATGTGTATAAGAGACAGGGGGTAATAGTGGGAGTGAGATATAAG
Cas9 ^ generation cutting assay FP	GTTGGGAAGGTGGAAGCTCA
Cas9 1st generation cutting assay RP	AGGATGCTAGGACAGCAGGA
Cas9 2nd and 3rd generation cutting assay FP	TCGTCGGCAGCGTCAGATGTGTATAAGAGACAGACTCACGTCATCCAGCAGAG
Cas9 2nd and 3rd generation cutting assay RP	GTCTCGTGGGCTCGGAGATGTGTATAAGAGACAGTTCACACGGCAGGCATACTC
B2M_Cas9_g1	CGCGAGCACAGCTAAGGCCA
B2M_Cas9_g2	ACTCTCTCTTTCTGGCCTGG
B2M_Cas9_g3	TCACGTCATCCAGCAGAGAA

B2M_Cas9_g4	CAGTAAGTCAACTTCAATGT
B2M_Cas9_g5	ATACTCATCTTTTTCAGTGG
B2M_Cas9_g6	AGTCACATGGTTCACACGGC
B2M_Cas9_g7	ACAAAGTCACATGGTTCACA
B2M_Cas9_g8	TGGGCTGTGACAAAGTCACA
B2M_Cas9_g9	GAGACATGTAAGCAGCATCA
B2M_Cas9_g10	ACATGTAAGCAGCATCATGG
B2M_Cas9_g11	GAATTCATCCAATCCAAATG
B2M_Cas9_g12	CATGTTTGATGTATCTGAGC
B2M_Cas9_g13	AGCCCTCCTAGAGCTACCTG
B2M_Cas9_g14	GTTGCTCCACAGGTAGCTCT
B2M_Cas9_g15	GCTCCACAGGTAGCTCTAGG
B2M_Cas9_g16	GAGGGCTGGCAACTTAGAGG
B2M_Cas9_g17	AGGGCTGGCAACTTAGAGGT
B2M_Cas9_g18	GGGCTGGCAACTTAGAGGTG
B2M_Cas9_g19	ATACTCTGCTTAGAATTTGG
B2M_Cas9_g20	GATAAAGTAAGGCATGGTTG
B2M_Cas9_g21	CACGCGTTTAATATAAGTGG
B2M_Cas9_g22	GGGCACGCGTTTAATATAAG
B2M_Cas9_g23	TATAAGTGGAGGCGTCGCGC
B2M_Cas9_g24	AAGTGGAGGCGTCGCGCTGG

B2M_Cas9_g25	AGTGGAGGCGTCGCGCTGGC
Cas9 crRNA 4 sequence	/5ThioMC6- UrArUrGrCrUD/iSp18/rCrArGrUrArArGrUrCrArArCrUrUrCrArArUrGrUrGrUrUrUrUrArGrArGrCr
B2M_Cas9_crRNA+ATTO488	/5ThioMC6- D//iSp18/rGrArArGrUrUrGrArCrUrUrArCrUrGrArArGrArArGrUrUrUrUrArGrArGrCrUrArUrGrCrU/3ATTO488N/
Modified gRNA for AuNP formulation B2M Cas12a crRNA sequence	rUrArArUrUrUrCrUrArCrUrCrUrUrGrUrArGrArUrArUrArUrArArGrUrGrGrArGrGrCrGrUrCrGrCrGrC/iSp18//3ThioMC3-D/
Modified gRNA for AuNP formulation B2M MG29-1 crRNA sequence	5'Thio-PEG_5-GUUGAGAAUCGA-nNtlinker- AAGAUUCUCAACCUUUUAAUUUCUACUGUUGUAGAUAGUGGGGGUGAAUUCAGUGU*mA*mG

Chapter 3: Discussion

The development of the 3rd generation CRISPR-AuNP represents a significant advancement in the ease of synthesis, stability of the formulation and modest advancement in the non-viral delivery of CRISPR RNP complexes to primary human HSPCs. This chapter expands on the findings from Chapter 2, situating the technology within the broader landscape of gene editing delivery systems and proposing future improvements to enhance its therapeutic potential. Specifically, we describe subsequent optimization steps, including antibody conjugation for active targeting (Appendix 1) and in vivo delivery of CRISPR-AuNP in an immunocompetent mouse model to evaluate efficacy and safety (Appendix 2). Additional optimization measures are also discussed.

3.1 3rd Generation CRISPR-AuNP Relative to the Field of Non-viral CRISPR Delivery Demonstrates Potential Utility

The systematic optimization from 1st to 3rd generation CRISPR-AuNP addressed several critical limitations in Cas9 loading, endosomal escape, and editing efficiency. The 1st generation formulation exhibited poor Cas9 RNP stability due to low pH conditions that disrupted the crRNA/trRNA duplex, resulting in negligible gene editing. This problem was exacerbated by the sequential loading approach, wherein the complete saturation of the AuNP core surface with RNA sterically hindered nuclease binding.

The 2nd generation improved RNP loading by pre-forming complexes prior to conjugation with the AuNP core, but the volume of AuNP core surface still exposed rendered PEI-coated

particles unstable. We then demonstrate that thiolated PEGylated PEI can occupy exposed AuNP core surface resolves this instability. However, the quantity of polymeric coating achieved by this method is insufficient to mediate endosomal escape. The 3rd generation addressed these issues by directly conjugating the polyplex to AuNP core. Optimization of the quantity of PEG-SH grafted demonstrated that P20PSH at 2 N/P ratio, achieved 13.23 ± 0.12% indels at the B2M gene in primary human HSPCs without compromising cell viability. Although this efficiency falls short of electroporation of RNP at the same dose (~40-45%), it provides a simpler, equipment-free alternative at a cost of less than $70 per million cells treated.

This platform could also load alternative CRISPR systems Cas12a and MG29-1 without requiring nuclease-specific engineering, and these systems demonstrated similar levels of activity (>10% gene editing) in primary human HSPC[101]. This versatility positions 3rd generation CRISPR-AuNP as a flexible tool for delivering diverse CRISPR systems, including next-generation editors like prime editors[21], which rely on extended gRNAs compatible with our thiol-based conjugation strategy. Nevertheless, the current editing efficiency remains below the therapeutic threshold (typically ≥20% for HSPC-based therapies), necessitating further refinement. However, Zeng and colleagues have recently described levels of editing <10% in unstimulated HSPC are sufficient to achieve therapeutic value in the treatment of sickle cell disease and maintain preserved engraftment owing to fewer off-target genotoxic events[53]. While HPSC in our study were cultured for 24 hours prior to treatment with 3rd

generation CRISPR-AuNP, if similar levels of editing are observed in unstimulated HSPC, the utility of this platform could be more readily translatable.

When compared to current clinical electroporation methods, our 3rd generation CRISPR-AuNP offers a simpler alternative[33]. Treatment simply involves adding the liquid nanoformulation to cells in standard culture conditions, with cell entry occurring within 6 hours as confirmed by confocal microscopy. This simplicity significantly reduces processing complexity and specialized equipment requirements.

The liquid formulation of fully prepared 3rd generation CRISPR-AuNP demonstrates favorable stability characteristics. When fully prepared, the nanoparticles remain stable and functional for up to 48 hours when stored at 4°C, though extended stability testing beyond this timepoint has not been conducted. Individual cargo components exhibit significantly greater stability: Cas9 RNP complexes maintain activity for approximately 2 weeks at 4°C, while the P20PSH polymer and AuNP cores can be stored for months at 4°C without degradation. This enables a modular preparation approach where components are maintained separately and assembled shortly before cellular treatment—preserving maximum editing efficiency while allowing advance preparation of complex components.

Compared to electroporation, this represents a significant advantage in workflow flexibility. Electroporation protocols require stringent timing between RNP preparation and cell processing, with narrow windows for optimal efficiency. Cells must be processed immediately

after electroporation in specialized recovery media to minimize toxicity and maximize viability. In contrast, our CRISPR-AuNP system accommodates more flexible scheduling, with components prepared in advance and assembled within hours of treatment.

In the broader field of non-viral CRISPR delivery, lipid nanoparticles (LNPs) have gained prominence due to their success in mRNA vaccine delivery. LNP typically deliver CRISPR components as mRNA or plasmids, facing challenges in HSPCs due to their inherently regulated translational activity and sensitivity to amino acid levels[51]. Although recent LNP formulations have achieved editing efficiencies of 30–40% in cell lines, their performance in primary HSPCs remains less consistent. Moreover, LNPs deliver mRNA instead of RNP complexes, which can result in more off-target effects in CRISPR applications[104]. Our CRISPR-AuNP system, by delivering pre-formed RNP complexes, bypasses these barriers and demonstrates no toxicity at 100 pmol doses.

Engineered virus-like particles (eVLPs) represent an advanced delivery platform for gene editing. Raguram et al.[105] developed eVLPs with evolved capsids, incorporating base editors or Cas9 fused to Gag proteins for packaging into retroviral-like particles. This approach requires complex protein expression in mammalian cells and purification via ultracentrifugation and chromatography. While achieving 60-80% editing efficiency in immortalized cell lines, their efficiency in primary HSPCs ranged from 20-30%. Similarly, the Peptide-enabled RNP Delivery for CRISPR Editing (PERC) system developed by Sahu et. al.[81] requires direct addition of cell-penetrating peptides to cell culture along with CRISPR

RNP. This approach demonstrated 10-20% editing in HSPCs but was toxic even at low concentrations. Additionally, both eVLPs and PERC systems require stringent cold-chain storage (−80°C for eVLPs, −20°C for PERC-modified proteins), whereas our individual CRISPR-AuNP components maintain stability at 4°C for weeks to months.

3.2 Optimization Strategies to Advance 3rd Generation CRISPR-AuNP

To advance the 3rd generation CRISPR-AuNP toward clinical relevance, we propose several enhancement strategies targeting key steps in the delivery pathway. The mechanism of CRISPR-AuNP cellular delivery involves natural endocytosis, endosome formation, polymer-mediated endosomal escape, and nuclear trafficking via the nuclear localization signals (NLS) present on the RNP complex (Figure. 18). Interventions at each of these steps could potentially enhance overall gene editing efficiency.

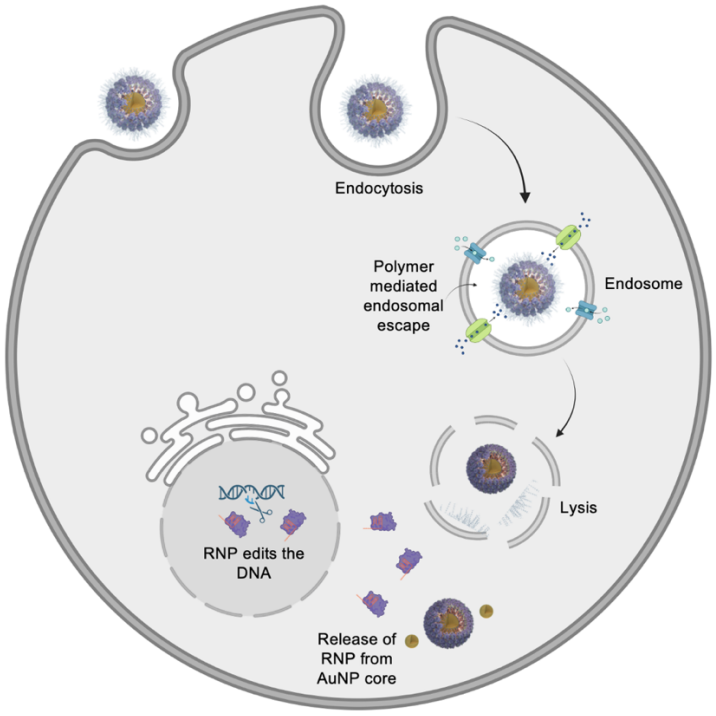

Figure. 18 | Mechanism of CRISPR-AuNP cellular entry and processing.

Schematic representation of 3rd generation CRISPR-AuNP internalization pathway in HSPCs. The diagram illustrates key steps: (1) endocytosis of the nanoparticle, (2) endosome formation, (3) polymer-mediated endosomal escape via proton sponge effect, (4) cytoplasmic release of cargo, and (5) nuclear translocation via NLS sequences present on the RNP complex.

3.2.1 Antibody targeting (Appendix 1)

HSPCs' basal endocytosis offers a passive entry route for nanoparticles, but their rarity (<1% of bone marrow cells)[47] and overlapping surface markers with other cell types complicate in vivo specificity[106]. Furthermore, there are multiple endosomal pathways which can be engaged using targeting moieties[31].

Since the 3rd generation CRISPR-AuNP described here includes covalent attachment of all cargo to the AuNP core, we tested whether conjugating antibodies targeting HSPC-specific receptors to the 3rd generation CRISPR-AuNP surface could increase uptake and editing efficiency[107]. Here we tested the ability to conjugate αCD90 to the 3rd generation formulation. The reason for choosing αCD90 is because of its targeting potential to HSPC shown by multiple groups[107,108].

Three potential strategies exist for antibody conjugation to CRISPR-AuNP: (1) electrostatic interaction, which is the simplest but least stable approach; (2) thiol-mediated covalent conjugation utilizing the thiols present on the antibody heavy and light chains, similar to

methods established by the Anderson group[109]; and (3) amine-mediated covalent conjugation using maleimide chemistry, which offers the highest stability but greatest complexity. We initiated our investigations with thiol-mediated conjugation, reducing αCD90 to expose thiols using tris(2-carboxyethyl)phosphine (TCEP). We confirmed antibody reduction into separate light and heavy chains via SDS-PAGE (Figure. 21) and verified that TCEP-reduced αCD90 maintained antigen recognition capability through biolayer interferometry (BLI) (Figure. 22).

CD90-conjugated 3rd generation CRISPR-AuNPs demonstrated modestly higher (Figure. 23) gene editing levels (16.08 ± 3.97%) compared to untargeted 3rd generation CRISPR-AuNP (13.23 ± 0.12%). While this improvement was not statistically significant, it suggests that receptor-mediated endocytosis can enhance CRISPR-AuNP uptake and editing outcomes as the pathways used for internalization differs from regular endocytosis uptake[109].

Future iterations could explore alternative targeting strategies, such as CD117 or CD133 antibodies, which may provide more selective HSPC targeting[1], particularly in the context of in vivo applications. Additionally, optimizing antibody loading density and orientation on the nanoparticle surface could further enhance targeting efficiency. Finally, more in-depth investigation of the endosomal biology used by HSPCs in vivo versus in vitro would facilitate identification of possible strategies to improve uptake and escape.

3.2.2 Endosomal Escape Enhancement

Following cellular internalization of CRISPR-AuNP, the polymer component facilitates the proton sponge effect[110], disrupting the endosomal membrane and releasing the nanoparticle contents. Our observations indicate that increasing PEG-SH concentration on the polymer correlates with enhanced gene editing efficiency, suggesting that further increases in PEG-SH content might continue this trend. The limitation in our studies to 20% PEG-SH grafting was due to commercial synthesis constraints. Development of novel synthetic methods to achieve higher PEG-SH grafting percentages would enable testing of whether this correlation persists at higher modification levels.

3.2.3 Nuclear Trafficking Optimization

CRISPR nucleases contain Nuclear Localization Signals (NLS) that facilitate their trafficking to the nucleus. Previous studies have demonstrated that increasing NLS density on nucleases can enhance nuclear localization and subsequently improve gene editing efficiency[111]. The nucleases employed in our studies contain two NLS domains. Future optimization experiments should evaluate the impact of additional NLS motifs on editing efficiency.

3.3 Potential for clinical translation

3.3.1 Preliminary in vivo data (Appendix 2)

A future goal of CRISPR-AuNP development is to enable in vivo editing of HSPCs, potentially circumventing the need for ex vivo manipulation. Appendix 2 presents preliminary

data from intravenous injection of 3rd generation Cas9 CRISPR-AuNP targeting the murine B2M gene into immunocompetent C57BL/6 mice. We screened 20 gRNAs using the previously described method for human B2M gRNA screening mentioned in chapter 2, targeting B2M for activity in MC-38 cells, a murine cell line derived from mouse colon, and identified gRNA 13 as the most efficient gRNA and used it as a target for murine studies (Figure. 24). We then assembled 3rd generation CRISPR-AuNP with cargo including gRNA 13 and Cas9 as described in Chapter 2.

We compared 3rd generation unpurified CRISPR-AuNP (1.92 mg/kg RNP, 10 mg/kg AuNP), 3rd generation purified CRISPR-AuNP (0.96 mg/kg RNP, 10 mg/kg AuNP), and polyplex-only controls (1.92 mg/kg RNP) by administering intravenously as a series of two injections at 1 injection per day for a total of 2 days (Figure. 25). Three days after first injection was administered, mice were euthanized and organs were harvested. Genomic DNA was isolated from various tissues and Indels at the B2M gene were quantified by DNA sequencing and analysis using CRISPRESSO, to assess in vivo efficacy. The unpurified formulation showed the highest editing efficiencies: 3.29 ± 2.18% in lungs, 1.73 ± 1.36% in thymus, 0.93 ± 0.76% in spleen, and 0.88 ± 1.45% in heart, with peak editing reaching 6.22% in lungs and 4.49% in thymus in individual mice (Figure. 26). The purified formulation, despite containing half the RNP dose, maintained similar editing levels in key tissues (1.55 ± 0.37% in thymus, 1.20 ± 0.46% in lungs), suggesting improved per-molecule efficiency. In the field, lipid nanoparticles (LNPs) are considered the gold standard for in vivo delivery due to their efficiency, although they predominantly accumulate in the liver. In contrast, our CRISPR-AuNP formulation

demonstrated broader biodistribution, with measurable editing across multiple organs, suggesting a potential advantage over LNPs in achieving systemic gene editing[101].

Importantly, acute inflammatory responses Interleukin -2 (IL-2), Interleukin (IL-6), Interferon – γ (IFN- γ), Tumor Necrosis Factor – α (TNF- α) and liver toxicity markers alanine aminotransferase (ALT) and aspartate aminotransferase (AST), measured at necropsy showed no significant elevations (Figure. 27) compared to mock-treated controls, indicating tolerability of the formulations at these doses, routes and schedule of administration. This safety profile aligns with our in vitro observations, supporting the biocompatibility of the platform, but long-term effects were not evaluated in this study, including development of immune responses to the CRISPR components.

While these in vivo editing efficiencies fall below therapeutic thresholds for most applications, they represent an encouraging starting point for a non-targeted nanoparticle system. Future development could incorporate active targeting moieties (as explored in Appendix 1) and optimized dosing regimens and routes of administration to enhance HSPC-specific delivery[46]. Additionally, assessing the persistence of edits through secondary transplantation studies would provide insights into the durability of genetic modifications in long-term repopulating stem cells[82].

3.3.2. Lyophilization of 3rd generation CRISPR-AuNP

We investigated lyophilization as a potential strategy for long-term storage of fully assembled particles. Preliminary experiments incorporating trehalose (10%) as a cryoprotectant[112] during the lyophilization process demonstrated successful reconstitution (Figure. 19A) and retention of activity in the MC38 cell line when targeting the murine B2M gene, with editing efficiency assessed by T7E1 assay (Figure. 19B). These initial results suggest potential for room-temperature storage of lyophilized CRISPR-AuNP formulations, though further optimization and comprehensive stability testing will be required.

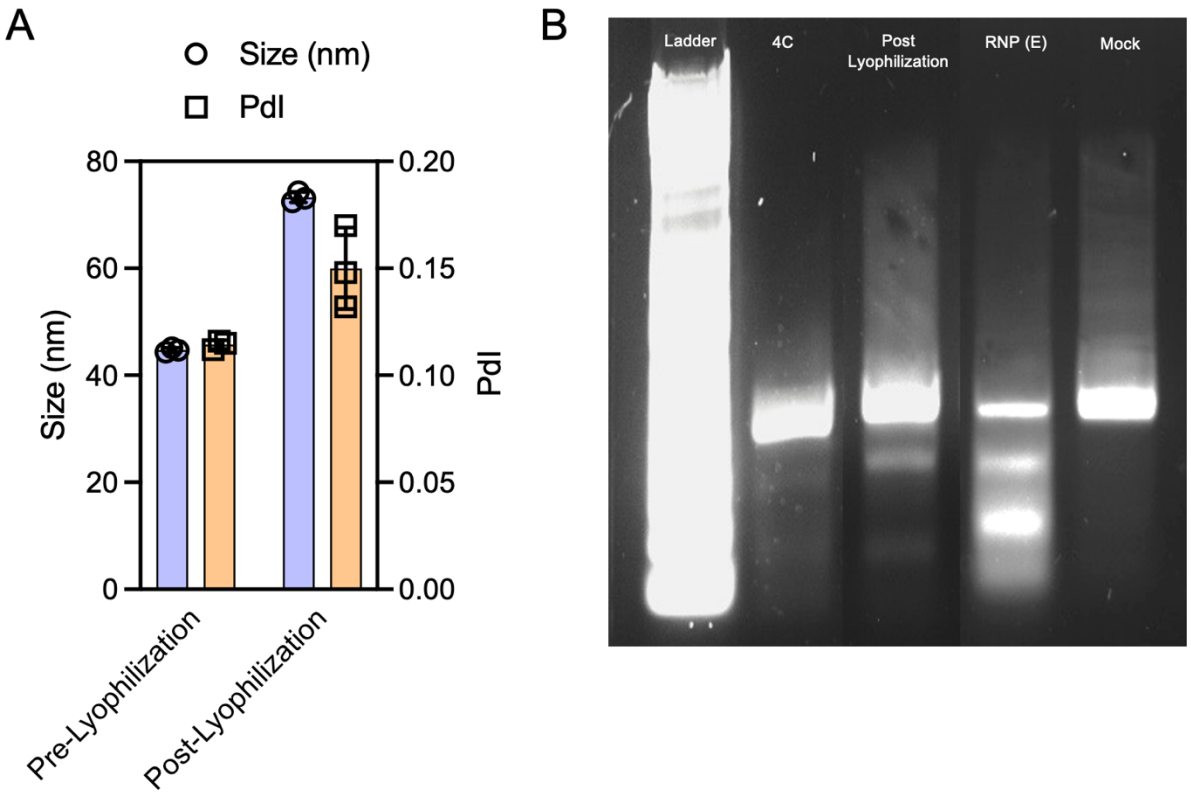

Figure. 19 | Lyophilized 3rd generation CRISPR-AuNP maintains stability and activity.

A) DLS measurements of 3rd generation CRISPR-AuNP formulated with Cas9 nuclease before and after lyophilization with 10% trehalose as cryoprotectant. Data are means ± SEM (n=3 technical replicates). B) T7E1 assay of B2m gene editing in MC38 cells. Lane 1: DNA ladder; Lane 2: Cells treated with pre-lyophilization CRISPR-AuNP; Lane 3: Cells treated with reconstituted post-lyophilization CRISPR-AuNP; Lane 4: Positive control - RNP electroporation; Lane 5: Mock treatment.

3.3 Conclusion

The 3rd generation CRISPR-AuNP advances non-viral CRISPR delivery by combining affordability, modularity, and moderate gene editing efficiency in HSPCs. While it does not yet match electroporation's potency for ex vivo applications or LNPs' systemic reach for in vivo delivery, its unique strengths—rapid assembly, RNP compatibility, low toxicity, and adaptability across CRISPR systems—distinguish the platform as highly usable and support additional refinements.

The appendices outlined address targeting specificity and in vivo performance. By bridging gaps in accessibility and adaptability, CRISPR-AuNP contributes to the democratization of gene editing technologies, potentially expanding the reach of precision genetic medicines to regions and populations with limited access to specialized facilities and equipment.

Future work should focus on enhancing targeting specificity through optimized antibody conjugation, improving in vivo delivery through formulation refinements such as alternative polymers or higher grafting levels of PEG-SH, and exploring applications with larger MW next-generation CRISPR systems such as base and prime editors. Additionally, investigating the platform's utility for delivering other therapeutic cargos, such as antisense oligonucleotides or short interfering RNAs, could expand its versatility beyond genome editing applications.

In summary, the 3rd generation CRISPR-AuNP represents a significant step forward in non-viral CRISPR delivery to HSPCs. By systematically addressing the physicochemical challenges of loading and delivering Cas9 RNP via gold nanoparticles, we have developed a platform that achieves meaningful gene editing without compromising cell viability. The system's modularity across multiple CRISPR nucleases positions it as a versatile tool for various gene editing applications, with substantial potential for further optimization toward therapeutic relevance.

Appendix 1: Antibody-Targeted CRISPR-AuNP

Introduction

The 3rd generation CRISPR-AuNP showed 13.23 ± 0.12% indels at the B2M gene in vitro in HSPCs, as detailed in Chapter 2. To enhance gene editing efficiency, we explored antibody-mediated targeting to improve cellular uptake. Antibody-driven endocytosis follows distinct pathways compared to the passive endocytosis of untargeted CRISPR-AuNP, potentially increasing delivery specificity and efficacy. Here, we conjugated a CD90 antibody to the 3rd generation CRISPR-AuNP by denaturing the antibody with Tris(2-carboxyethyl)phosphine

(TCEP) to expose thiol groups, which were then integrated into the polyplex and linked to the AuNP surface.

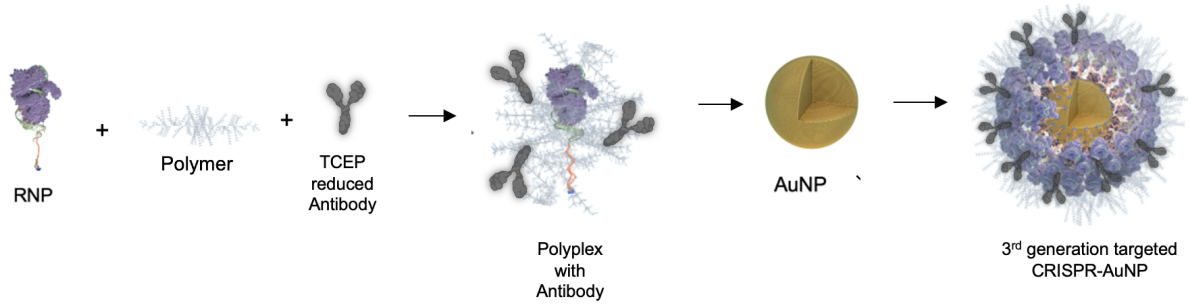

Figure 20 | Preparation workflow for antibody-targeted 3rd generation CRISPR-AuNP.

Schematic representation of the synthesis process for CD90-targeted 3rd generation CRISPR-AuNP.

Results

Binding Specificity of Denatured CD90

BLI analysis confirmed that TCEP-denatured CD90 retained binding specificity comparable to the undenatured positive control, indicating that denaturation did not compromise its targeting capability.

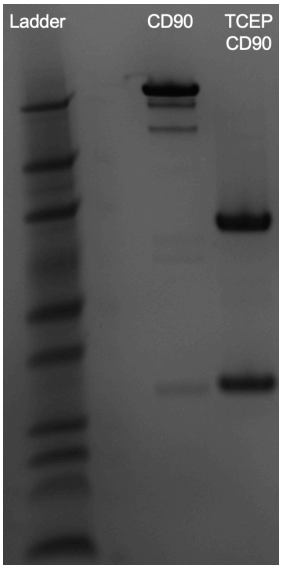

Figure 21 | TCEP treatment reduces CD90 antibody into component chains.

SDS-PAGE analysis of CD90 antibody before and after TCEP treatment. Lane 1: Protein ladder; Lane 2: Untreated CD90 antibody; Lane 3: TCEP-reduced CD90 antibody showing separated heavy and light chains.

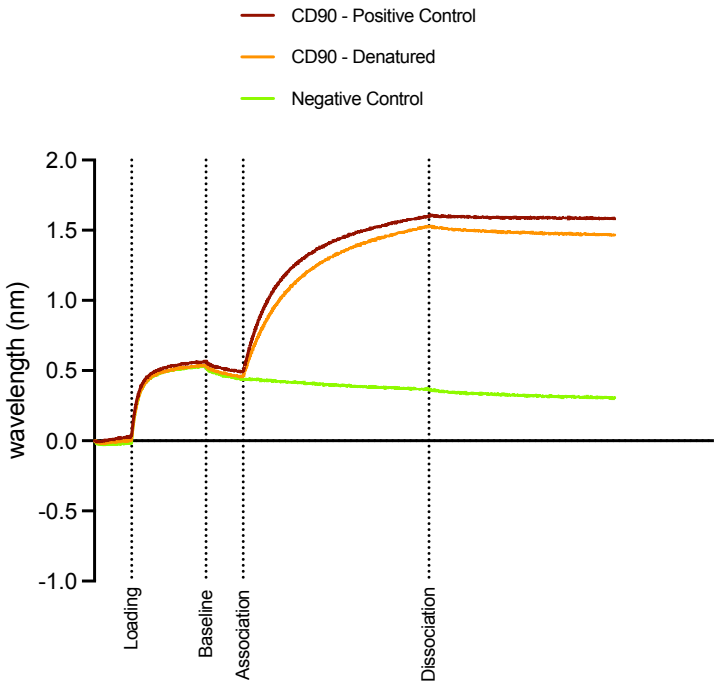

Figure 22 | TCEP-reduced CD90 antibody maintains antigen binding capacity.

Biolayer interferometry (BLI) sensor grams showing binding kinetics of CD90 antibody to immobilized antigen. Y-axis represents binding response (nm); X-axis shows time (seconds). Both association and dissociation phases are displayed.

Gene Editing and B2M Knockdown

CD90-targeted CRISPR-AuNP were synthesized by incorporating 25 pmol of denatured CD90 into the polyplex prior to AuNP conjugation. In CD34+ HSPCs, CD90-targeted CRISPR-AuNP increased B2M knockdown compared to non-targeted counterparts, though the difference was not statistically significant. Gene editing efficiency, measured as indel frequency at the B2M gene, averaged 16.08 ± 3.97% for CD90-targeted CRISPR-AuNP versus 13.23 ± 0.12% for non-targeted controls, suggesting a modest improvement. Cell viability remained unaffected across all conditions, consistent with mock-treated controls.

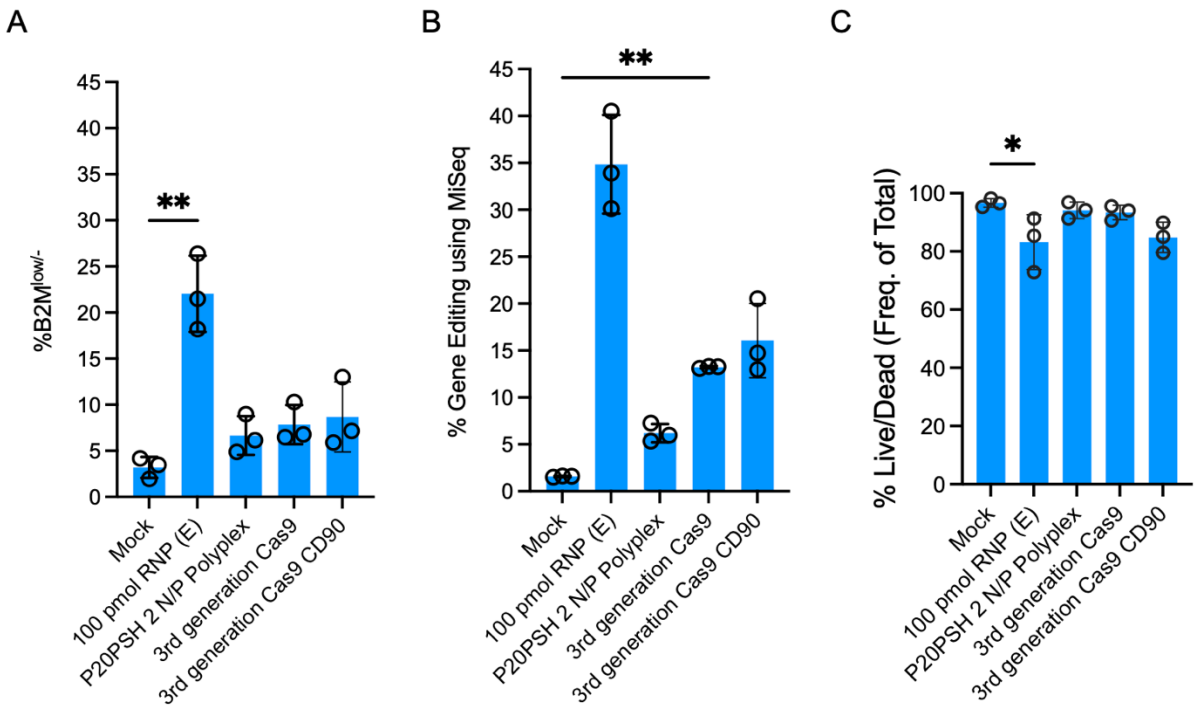

Figure 23 | CD90-targeted 3rd generation CRISPR-AuNP enhances gene editing in HSPCs.

A) Percentage of B2M$^{low/-}$ cells in CD34+ HSPCs treated with various formulations, measured by flow cytometry. B) Indel frequency at the B2M gene determined by DNA sequencing. C) Cell viability assessed by live/dead staining. Measurements performed 72 hours post-treatment. Data are means ± SD (n=3 biological replicates).

Discussion

Conjugation of CD90 to the 3rd generation CRISPR-AuNP modestly enhanced gene editing and B2M knockdown in HSPCs, likely due to improved uptake via receptor-mediated endocytosis. The lack of statistical significance may reflect variability across replicates or

suboptimal CD90 loading (25 pmol). BLI confirmed that denaturation preserved CD90 specificity, validating the conjugation approach. Compared to electroporation, targeted CRISPR-AuNP underperformed, but they outperformed polyplexes alone, highlighting the AuNP's role in delivery enhancement. Future experiments should employ confocal microscopy to confirm intracellular trafficking and test alternative antibodies (e.g., CD133, CD117) to optimize targeting efficiency.

Appendix 2: In vivo safety and efficacy of 3rd gen CRISPR-AuNP

In Chapter 2, we developed the 3rd generation CRISPR-AuNP, optimized for human HSPCs in vitro. Using pre-formed Cas9 RNP and thiolated poly(ethyleneimine)-poly(ethylene glycol) (P20PSH) polymer at a 2 N/P ratio, we achieved 13.23 ± 0.12% indels at the B2M gene, with no viability loss and cell entry within 6 hours, outperforming polyplexes (6.19 ± 0.97%) and extending to Cas12a (15.07 ± 1.9%) and MG29-1 (13.39 ± 1.5%). Costing less than $70 per

million cells, this platform offers a simpler alternative to electroporation and LNPs. Here, we evaluate its in vivo performance in C57Bl/6 mice, targeting the murine B2m gene—a quantifiable marker of editing efficiency and biodistribution. We assessed editing across tissues, with a focus on bone marrow, and safety through cytokine and liver enzyme profiles, comparing unpurified and purified formulations against polyplex controls to advance this platform toward therapeutic in vivo use.

Results

Selection of Murine B2m gRNA for In Vivo Studies

To adapt the 3rd generation CRISPR-AuNP for in vivo use, we screened gRNAs targeting B2m using the GRCm39/mm39 assembly, mirroring Chapter 2's approach. The top 20 gRNAs were electroporated into MC38 cells (100 pmol RNP), with editing assessed by flow cytometry (B2M loss) and sequencing. Cas9 gRNA 13 (g13) yielded 48.5 ± 12.3% $B2M^{low/-}$ cells and 52.1 ± 14.7% indels (n=3) (Figure. 24), comparable to Chapter 2's 47.8 ± 15.3% at human B2M, and was selected for its robust performance.

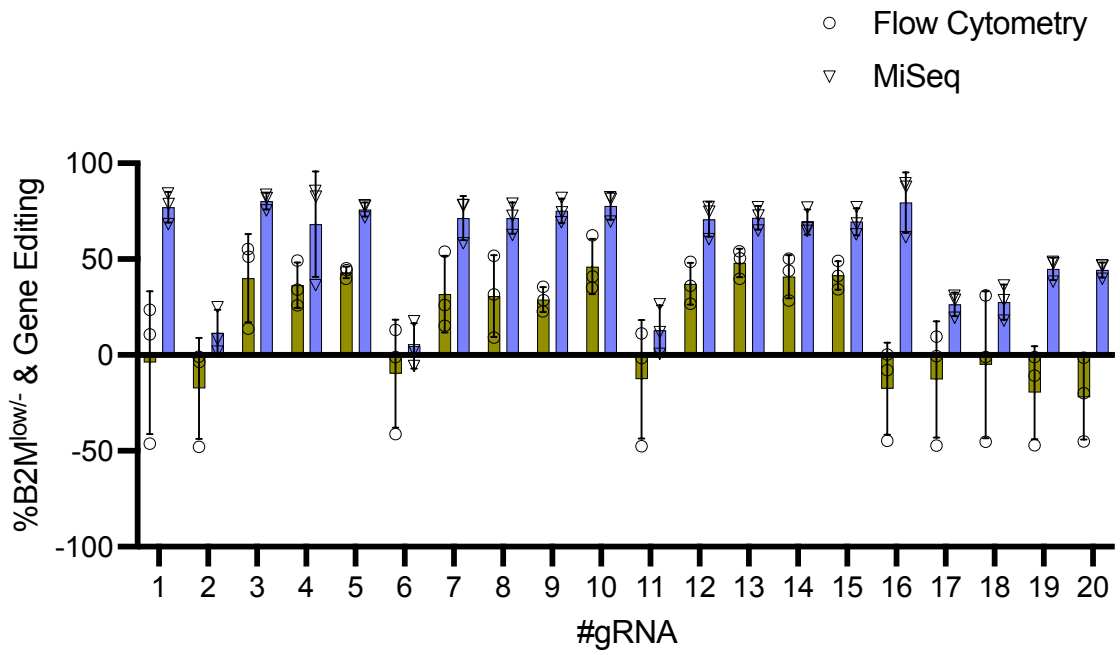

Figure 24 | Screening of gRNAs targeting murine B2m in MC38 cells.

Flow cytometry and MiSeq sequencing analysis of B2m editing in MC38 cells electroporated with Cas9 RNP complexes containing different candidate gRNAs targeting the B2m gene. Left bars: percentage of $B2M^{low/-}$ cells determined by flow cytometry. Right bars: percentage of edited reads (indels within 40 bp of predicted cut sites) quantified by MiSeq sequencing with CRISPRESSO analysis. Data are means ± SD (n=3 independent experiments).

In Vivo Gene Editing Efficiency Across Tissues

We administered the 3rd generation CRISPR-AuNP via tail vein injections in C57Bl/6 mice, n=8 per group: mock (untreated), unpurified (1.92 mg/kg RNP, 10 mg/kg AuNP), purified (0.96 mg/kg RNP, 10 mg/kg AuNP), and polyplex-only (1.92 mg/kg RNP). Doses were split over two days, 5 mg/kg AuNP per day, and mice were euthanized 72 hours post-final injection

(Figure. 25). Genomic DNA from blood, bone marrow, spleen, lungs, thymus, heart, and liver was analyzed for indels using CRISPRESSO[94]. The unpurified group showed the highest editing: 3.29 ± 2.18% in lungs, 1.73 ± 1.36% in thymus, 0.93 ± 0.76% in spleen, and 0.88 ± 1.45% in heart, with peak efficiencies reaching 6.22% in lungs and 4.49% in thymus in individual mice (Figure. 26). The purified group exhibited similar editing: 1.55 ± 0.37% in thymus and 1.20 ± 0.46% in lungs, with 0.51 ± 0.43% in bone marrow and 0.23 ± 0.20% in liver. The polyplex group demonstrated lower editing: 1.15 ± 1.07% in thymus, 0.25 ± 0.35% in lungs, and less than 0.5% elsewhere. Mock controls displayed indels below 0.1%. High editing in lungs and thymus reflects phagocytic uptake, while the 2.11% peak in bone marrow with the unpurified formulation suggests limited HSPC access.

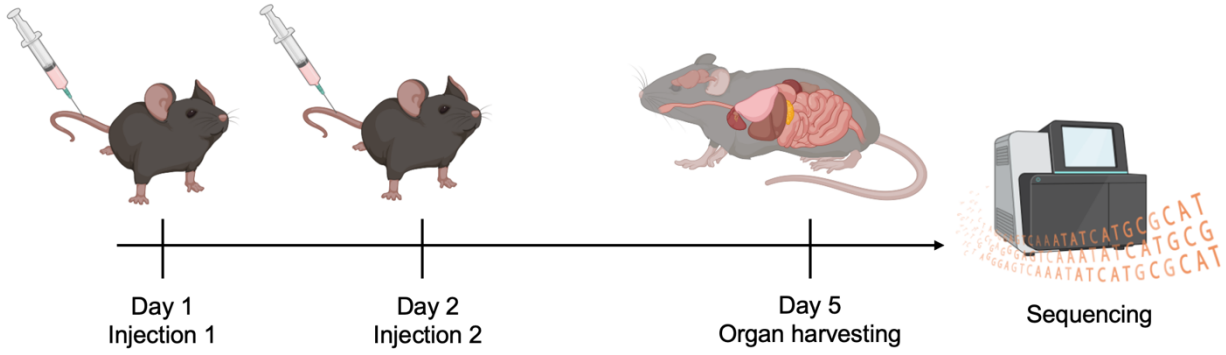

Figure 25 | Experimental design for in vivo evaluation of 3rd generation CRISPR-AuNP.

Schematic representation of the in vivo study timeline using C57BL/6 mice. Dosing schedule of tail vein injections (days 1-2), sacrifice timepoint (day 5), and analysis performed (tissue gene editing analysis, inflammatory markers, liver enzymes).

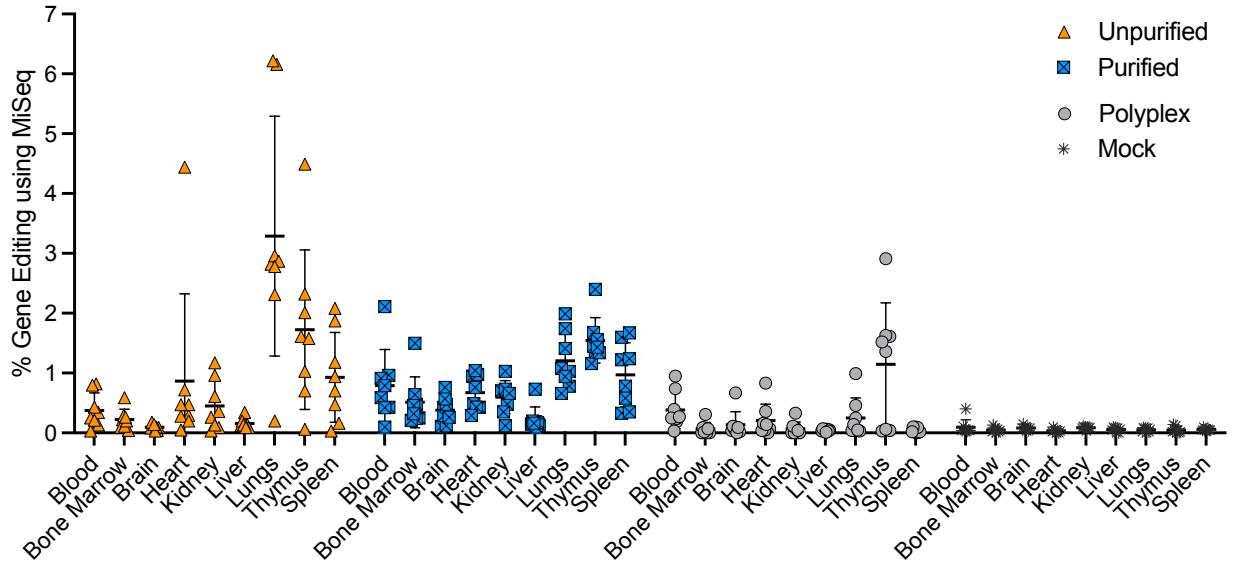

Figure 26 | Tissue distribution of gene editing after systemic 3rd generation CRISPR-AuNP administration.

Percentage of indels at the B2m gene across tissues in C57BL/6 mice (n=8 per group) 72 hours after the final injection of different formulations. Treatment groups: mock (untreated), unpurified CRISPR-AuNP (1.92 mg/kg RNP, 10 mg/kg AuNP), purified CRISPR-AuNP (0.96 mg/kg RNP, 10 mg/kg AuNP), and polyplex-only (1.92 mg/kg RNP). Data are means ± SD.

Inflammatory Responses and Hepatotoxicity

Safety was assessed via serum cytokines (IL-2, IL-6, IFN-γ, TNF-α) and liver enzymes (ALT, AST) 72 hours post-treatment. Cytokines showed slight elevations in the unpurified group with IL-6 at 15.2 ± 8.9 pg/mL and in the polyplex group with TNF-α at 12.7 ± 6.3 pg/mL, compared to the mock group with IL-6 at 8.1 ± 3.2 pg/mL and TNF-α at 7.4 ± 2.8 pg/mL, but differences were non-significant, $p > 0.05$, ANOVA (Figure. 27). ALT and AST levels were higher in the unpurified group with ALT at 35.6 ± 12.4 U/L and AST at 82.3 ± 19.7 U/L, and in the polyplex group with ALT at 33.9 ± 10.8 U/L and AST at 79.5 ± 15.6 U/L, compared to the mock group with ALT at 28.7 ± 9.1 U/L and AST at 70.2 ± 13.4 U/L, yet these were also non-significant, $p > 0.05$ (Figure. 27). This aligns with Chapter 2's minimal in vitro toxicity.

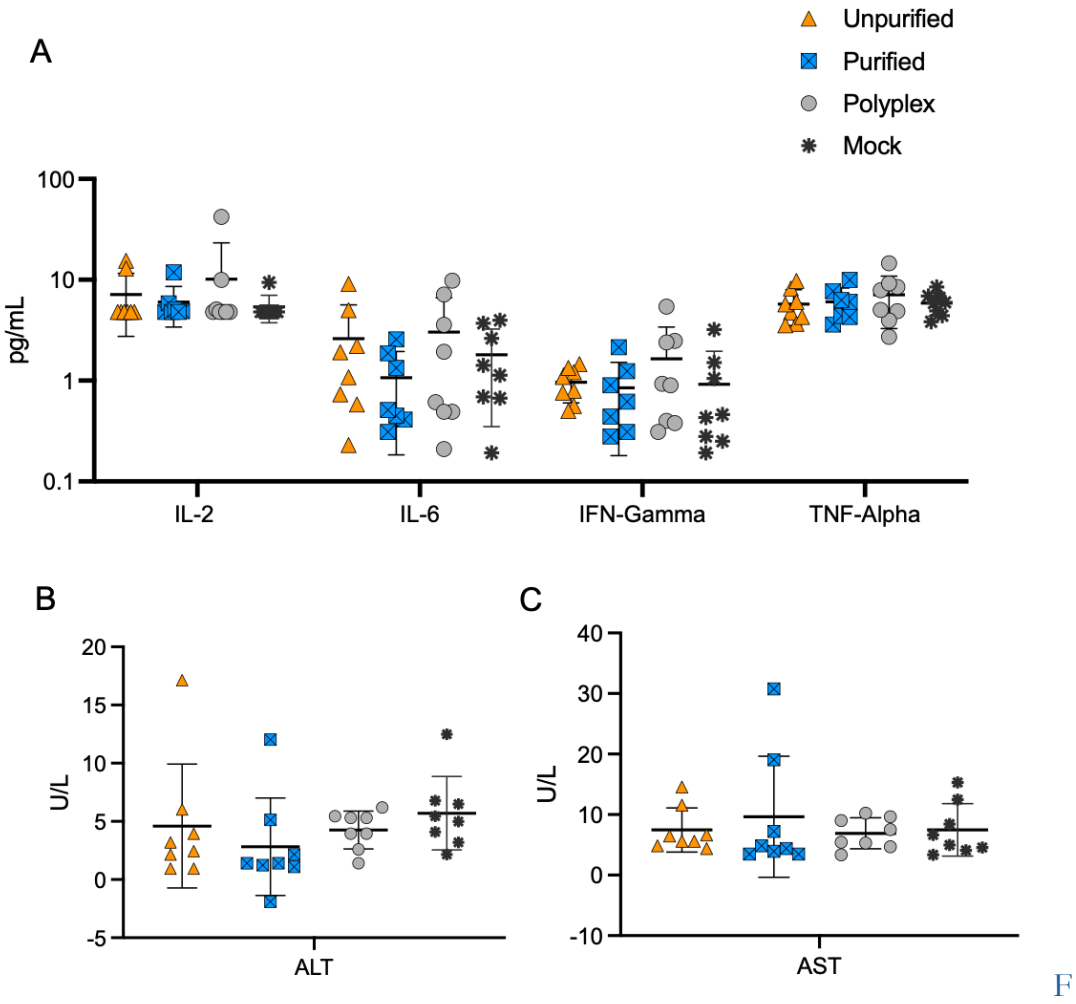

Figure. 27 | No significant Inflammatory and Hepatotoxicity Profiles following 3rd Generation CRISPR-AuNP Administration at necropsy

A) Serum cytokine concentrations (pg/mL) of IL-2, IL-6, IFN-γ, and TNF-α in C57BL/6 mice (n=8 per group) 72 hours after tail vein injection of different formulations, measured via Luminex assay. B) Liver enzyme levels (U/L) of ALT and AST. Treatment groups: mock (untreated), unpurified CRISPR-AuNP (1.92 mg/kg RNP, 10 mg/kg AuNP), purified CRISPR-AuNP (0.96 mg/kg RNP, 10 mg/kg AuNP), and polyplex-only (1.92 mg/kg RNP). Data are means ± SD

Discussion

This section extends Chapter 2's in vitro success with the 3rd generation CRISPR-AuNP to in vivo editing in mice, targeting B2m. We achieved peak editing in lungs (6.22%) and thymus (4.49%) with unpurified formulations, while purified versions sustained efficiency (thymus: 1.55 ± 0.37%) at half the RNP dose, with bone marrow at 2.11% maximum. Notably, the highest editing across all three formulations was observed in the thymus. The thymus contains a heterogeneous mix of phagocytic and epithelial cells, which may enhance nanoparticle uptake or retention. This observation warrants further investigation into organ-specific biodistribution and cellular uptake mechanisms. No significant cytokine or liver enzyme elevations were observed, consistent with Chapter 2's safety profile.

Compared to in vivo standards, our 1–6% editing is modest. AAVs achieve 20–30% in liver but <5% in bone marrow, while LNPs reach 15–40% in hepatocytes yet <5% in HSPCs without targeting. Breda et al.'s[46] CD117-LNPs edited ~90% of HSPCs in vivo, far surpassing our results, though requiring mRNA optimization and conditioning regimen. The unpurified formulation's advantage suggests excess RNP/polymer enhances delivery, while purification improves per-molecule efficiency.

3rd gen CRISPR-AuNP 13.23% in vitro editing drops in vivo due to systemic barriers (e.g., biodistribution, clearance), yet our platform's simplicity and cost (<$70/dose) remain strengths. Its modularity, proven with Cas12a and MG29-1, suggests broader in vivo potential. Future work could enhance HSPC targeting via CD117 conjugation, assess edit durability in secondary transplants, and evaluate off-target effects. While below therapeutic thresholds (e.g.,

≥20% for sickle cell disease), this platform advances non-viral CRISPR delivery, bridging Chapter 2 to in vivo applications.

Methods:

gRNA Selection and In Vitro Validation

B2M gRNAs were identified using GRCm39/mm39 and ranked. The top 20, synthesized were electroporated (100 pmol RNP) into MC38 cells. After 72 hours, cells were stained with PE-anti-B2M. DNA was extracted with quick extract, amplified, and sequenced to quantify indels (CRISPRESSO). Cas9 g13 was selected.

CRISPR-AuNP Synthesis and Administration

The 3rd generation CRISPR-AuNP was synthesized as in Chapter 2, using P20PSH (2 N/P) with Cas9 RNP (g13). Unpurified CRISPR-AuNP combined 10 μg AuNP cores (17 nm) with 100 pmol RNP-polyplexes (1.92 mg/kg RNP, 10 mg/kg AuNP). Purified CRISPR-AuNP underwent two centrifugation rounds (10,000 × g, 15 min), resuspending in PBS (0.96 mg/kg RNP, 10 mg/kg AuNP). Polyplexes (2 N/P P20PSH, 1.92 mg/kg RNP) were controls. C57Bl/6 mice (6 weeks, Jackson Laboratory) received tail vein injections (200 μL, 5 mg/kg AuNP mass) on days 1 and 2, euthanized on day 5 (CO_2, cardiac puncture).

Tissue Processing and Gene Editing Analysis

Organs were dissociated into single-cell suspensions, and DNA was extracted (Quick Extract – Biosearch Tech). The B2M gene was amplified (forward: 5'-

AGCTGGCTGAATGTTCTCC-3'; reverse: 5'-TGCAGTAGTTGTGGGAGATG-3'), sequenced (Illumina MiSeq), and indels quantified (CRISPRESSO v2.0.30).

Serum Cytokine and Liver Enzyme Assays

Serum was separated (2,000 × g, 10 min). Cytokines were quantified via Luminex 200 (25 µL, 1:2 dilution, 2-hour bead incubation, streptavidin-phycoerythrin). ALT and AST used RayBiotech kits. Data were analyzed (ANOVA, GraphPad Prism 9).

Table 3:

Murine B2m gRNA sequences

K/J/D_mB2M_sek_G1	GCTACTCGGCGCTTCAGTCG
K/J/D_mB2M_sek_G2	AGTCGTCAGCATGGCTCGCT
K/J/D_mB2M_sek_G3	GACAAGCACCAGAAAGACCA
K/J/D_mB2M_sek_G4	CTGGTGCTTGTCTCACTGAC
K/J/D_mB2M_sek_G5	AGTATACTCACGCCACCCAC
K/J/D_mB2M_sek_G6	GCTTCCCATTCTCCGGTGGG
K/J/D_mB2M_sek_G7	TCGGCTTCCCATTCTCCGGT
K/J/D_mB2M_sek_G8	GGATTTCAATGTGAGGCGGG
K/J/D_mB2M_sek_G9	ATTTGGATTTCAATGTGAGG
K/J/D_mB2M_sek_G10	AGCATTTGGATTTCAATGTG
K/J/D_mB2M_sek_G11	GGGTGAATTCAGTGTGAGCC

K/J/D_mB2M_sek_G12	GTATGTATCAGTCTCAGTGG
K/J/D_mB2M_sek_G13	CGTATGTATCAGTCTCAGTG
K/J/D_mB2M_sek_G14	GCGTATGTATCAGTCTCAGT
K/J/D_mB2M_sek_G15	GGCGTATGTATCAGTCTCAG
K/J/D_mB2M_sek_G16	CCAAGTAATGAGAAGTACAG
K/J/D_mB2M_sek_G17	AGAAGTAGCCACAGGGTTGG
K/J/D_mB2M_sek_G18	AGCAGAAGTAGCCACAGGGT
K/J/D_mB2M_sek_G19	CAAAAGCAGAAGTAGCCACA
K/J/D_mB2M_sek_G20	ACAAAAGCAGAAGTAGCCAC

References

1. Friedmann, T. & Roblin, R. Gene therapy for human genetic disease? Science 175, 949–955 (1972).
2. Naldini, L. Gene therapy returns to centre stage. Nature 526, 351–360 (2015).

3. Collins, F. S. & Gottlieb, S. The Next Phase of Human Gene-Therapy Oversight. N. Engl. J. Med. 379, 1393–1395 (2018).
4. Dunbar, C. E. et al. Gene therapy comes of age. Science 359, eaan4672 (2018).
5. High, K. A. & Roncarolo, M. G. Gene Therapy. N. Engl. J. Med. 381, 455–464 (2019).
6. Blaese, R. M. et al. T Lymphocyte-Directed Gene Therapy for ADA⁻ SCID: Initial Trial Results After 4 Years. Science 270, 475–480 (1995).
7. Fischer, A., Hacein-Bey-Abina, S. & Cavazzana-Calvo, M. 20 years of gene therapy for SCID. Nat. Immunol. 11, 457–460 (2010).
8. Kohn, D. B. et al. Lentiviral gene therapy for X-linked chronic granulomatous disease. Nat. Med. 26, 200–206 (2020).
9. Wilson, J. M. Lessons learned from the gene therapy trial for ornithine transcarbamylase deficiency. Mol. Genet. Metab. 96, 151–157 (2009).
10. Hacein-Bey-Abina, S. et al. Insertional oncogenesis in 4 patients after retrovirus-mediated gene therapy of SCID-X1. J. Clin. Invest. 118, 3132–3142 (2008).
11. Braun, C. J. et al. Gene therapy for Wiskott-Aldrich Syndrome-Long-term reconstitution and clinical benefits, but increased risk for leukemogenesis. Rare Dis. Austin Tex 2, e947749 (2014).
12. Williams, D. A. & Baum, C. Medicine. Gene therapy--new challenges ahead. Science 302, 400–401 (2003).
13. Li, L. & Mandal, P. K. Recent advancements in gene therapy for sickle cell disease and β-thalassemia. Front. Hematol. 3, 1468952 (2024).

14. Rueda, J., De Miguel Beriain, Í. & Montoliu, L. Affordable Pricing of CRISPR Treatments is a Pressing Ethical Imperative. CRISPR J. 7, 220–226 (2024).
15. https://globalgenes.org/raredaily/bluebird-withdraws-gene-therapies-in-europe-as-it-winds-down-operations-there/.
16. Ishino, Y., Shinagawa, H., Makino, K., Amemura, M. & Nakata, A. Nucleotide sequence of the iap gene, responsible for alkaline phosphatase isozyme conversion in Escherichia coli, and identification of the gene product. J. Bacteriol. 169, 5429–5433 (1987).
17. Jinek, M. et al. A Programmable Dual-RNA–Guided DNA Endonuclease in Adaptive Bacterial Immunity. Science 337, 816–821 (2012).
18. Gaj, T., Gersbach, C. A. & Barbas, C. F. ZFN, TALEN, and CRISPR/Cas-based methods for genome engineering. Trends Biotechnol. 31, 397–405 (2013).
19. Westermann, L., Neubauer, B. & Köttgen, M. Nobel Prize 2020 in Chemistry honors CRISPR: a tool for rewriting the code of life. Pflugers Arch. 473, 1–2 (2021).
20. Villiger, L. et al. CRISPR technologies for genome, epigenome and transcriptome editing. Nat. Rev. Mol. Cell Biol. 25, 464–487 (2024).
21. Anzalone, A. V., Koblan, L. W. & Liu, D. R. Genome editing with CRISPR–Cas nucleases, base editors, transposases and prime editors. Nat. Biotechnol. 38, 824–844 (2020).
22. Kleinstiver, B. P. et al. Genome-wide specificities of CRISPR-Cas Cpf1 nucleases in human cells. Nat. Biotechnol. 34, 869–874 (2016).
23. Hu, Y. et al. Metagenomic discovery of novel CRISPR-Cas13 systems. Cell Discov. 8, 107 (2022).

24. Lamothe, R. C. et al. Novel CRISPR-Associated Gene-Editing Systems Discovered in Metagenomic Samples Enable Efficient and Specific Genome Engineering. CRISPR J. 6, 243–260 (2023).
25. Komor, A. C. et al. Improved base excision repair inhibition and bacteriophage Mu Gam protein yields C:G-to-T:A base editors with higher efficiency and product purity. Sci. Adv. 3, eaao4774 (2017).
26. Yan, J., Cirincione, A. & Adamson, B. Prime Editing: Precision Genome Editing by Reverse Transcription. Mol. Cell 77, 210–212 (2020).
27. Yarnall, M. T. N. et al. Drag-and-drop genome insertion of large sequences without double-strand DNA cleavage using CRISPR-directed integrases. Nat. Biotechnol. 41, 500–512 (2023).
28. Gelsinger, D. R. et al. Bacterial genome engineering using CRISPR-associated transposases. Nat. Protoc. 19, 752–790 (2024).
29. Bendixen, L., Jensen, T. I. & Bak, R. O. CRISPR-Cas-mediated transcriptional modulation: The therapeutic promises of CRISPRa and CRISPRi. Mol. Ther. J. Am. Soc. Gene Ther. 31, 1920–1937 (2023).
30. Nuñez, J. K. et al. Genome-wide programmable transcriptional memory by CRISPR-based epigenome editing. Cell 184, 2503-2519.e17 (2021).
31. Tsuchida, C. A., Wasko, K. M., Hamilton, J. R. & Doudna, J. A. Targeted nonviral delivery of genome editors in vivo. Proc. Natl. Acad. Sci. 121, e2307796121 (2024).

32. Molaei, Z., Jabbarpour, Z., Omidkhoda, A. & Ahmadbeigi, N. Exploring non-viral methods for the delivery of CRISPR-Cas ribonucleoprotein to hematopoietic stem cells. Stem Cell Res. Ther. 15, 233 (2024).
33. Bak, R. O., Dever, D. P. & Porteus, M. H. CRISPR/Cas9 genome editing in human hematopoietic stem cells. Nat. Protoc. 13, 358–376 (2018).
34. Doulatov, S., Notta, F., Laurenti, E. & Dick, J. E. Hematopoiesis: A Human Perspective. Cell Stem Cell 10, 120–136 (2012).
35. Chandrakasan, S. & Malik, P. Gene therapy for hemoglobinopathies: the state of the field and the future. Hematol. Oncol. Clin. North Am. 28, 199–216 (2014).
36. To, L. B., Haylock, D. N., Simmons, P. J. & Juttner, C. A. The Biology and Clinical Uses of Blood Stem Cells. Blood 89, 2233–2258 (1997).
37. Adashi, E. Y., Gruppuso, P. A. & Cohen, I. G. CRISPR Therapy of Sickle Cell Disease: The Dawning of the Gene Editing Era. Am. J. Med. 137, 390–392 (2024).
38. Wilkinson, A. C. et al. Author Correction: Long-term ex vivo haematopoietic-stem-cell expansion allows nonconditioned transplantation. Nature 571, E12 (2019).
39. Frangoul, H. et al. CRISPR-Cas9 Gene Editing for Sickle Cell Disease and β-Thalassemia. N. Engl. J. Med. 384, 252–260 (2021).
40. Lino, C. A., Harper, J. C., Carney, J. P. & Timlin, J. A. Delivering CRISPR: a review of the challenges and approaches. Drug Deliv. 25, 1234–1257 (2018).
41. Choudhury, A. et al. High-depth African genomes inform human migration and health. Nature 586, 741–748 (2020).

42. Cancellieri, S. et al. Human genetic diversity alters off-target outcomes of therapeutic gene editing. Nat. Genet. 55, 34–43 (2023).
43. Doxzen, K. W. et al. The translational gap for gene therapies in low- and middle-income countries. Sci. Transl. Med. 16, eadn1902 (2024).
44. https://www.who.int/data/gho/data/indicators/indicator-details/GHO/general-availability-of-bone-marrow-transplantation-in-the-public-health-system.
45. Glausiusz, J. How to deliver sound science in resource-poor regions. Nature 559, 647–649 (2018).
46. Breda, L. et al. In vivo hematopoietic stem cell modification by mRNA delivery. Science 381, 436–443 (2023).
47. Laurenti, E. & Göttgens, B. From haematopoietic stem cells to complex differentiation landscapes. Nature 553, 418–426 (2018).
48. Radtke, S. et al. A distinct hematopoietic stem cell population for rapid multilineage engraftment in nonhuman primates. Sci. Transl. Med. 9, eaan1145 (2017).
49. Laurenti, E. & Dick, J. E. Molecular and functional characterization of early human hematopoiesis. Ann. N. Y. Acad. Sci. 1266, 68–71 (2012).
50. Watts, K. L., Adair, J. & Kiem, H.-P. Hematopoietic stem cell expansion and gene therapy. Cytotherapy 13, 1164–1171 (2011).
51. Mohrin, M. et al. Hematopoietic stem cell quiescence promotes error-prone DNA repair and mutagenesis. Cell Stem Cell 7, 174–185 (2010).
52. Aguadé-Gorgorió, J. et al. MYCT1 controls environmental sensing in human haematopoietic stem cells. Nature 630, 412–420 (2024).

53. Zeng, J. et al. Gene editing without ex vivo culture evades genotoxicity in human hematopoietic stem cells. Cell Stem Cell 32, 191-208.e11 (2025).
54. Yin, H. et al. Non-viral vectors for gene-based therapy. Nat. Rev. Genet. 15, 541–555 (2014).
55. Lin, Y., Wagner, E. & Lächelt, U. Non-viral delivery of the CRISPR/Cas system: DNA versus RNA versus RNP. Biomater. Sci. 10, 1166–1192 (2022).
56. Milone, M. C. & O'Doherty, U. Clinical use of lentiviral vectors. Leukemia 32, 1529–1541 (2018).
57. Ran, F. A. et al. In vivo genome editing using Staphylococcus aureus Cas9. Nature 520, 186–191 (2015).
58. Sheridan, C. CRISPR therapies march into clinic, but genotoxicity concerns linger. Nat. Biotechnol. 39, 897–899 (2021).
59. Uchida, N. et al. Cas9 protein delivery non-integrating lentiviral vectors for gene correction in sickle cell disease. Mol. Ther. - Methods Clin. Dev. 21, 121–132 (2021).
60. Wang, J.-H., Gessler, D. J., Zhan, W., Gallagher, T. L. & Gao, G. Adeno-associated virus as a delivery vector for gene therapy of human diseases. Signal Transduct. Target. Ther. 9, 78 (2024).
61. Colella, P., Ronzitti, G. & Mingozzi, F. Emerging Issues in AAV-Mediated In Vivo Gene Therapy. Mol. Ther. Methods Clin. Dev. 8, 87–104 (2018).
62. Yin, H. et al. Therapeutic genome editing by combined viral and non-viral delivery of CRISPR system components in vivo. Nat. Biotechnol. 34, 328–333 (2016).

63. Mingozzi, F. & High, K. A. Immune responses to AAV vectors: overcoming barriers to successful gene therapy. Blood 122, 23–36 (2013).
64. Li, C. et al. HDAd5/35++ Adenovirus Vector Expressing Anti-CRISPR Peptides Decreases CRISPR/Cas9 Toxicity in Human Hematopoietic Stem Cells. Mol. Ther. Methods Clin. Dev. 9, 390–401 (2018).
65. Li, C. et al. In Vivo HSC Gene Therapy Using a Bi-modular HDAd5/35++ Vector Cures Sickle Cell Disease in a Mouse Model. Mol. Ther. J. Am. Soc. Gene Ther. 29, 822–837 (2021).
66. Boucher, P., Cui, X. & Curiel, D. T. Adenoviral vectors for in vivo delivery of CRISPR-Cas gene editors. J. Control. Release Off. J. Control. Release Soc. 327, 788–800 (2020).
67. Hacein-Bey-Abina, S. et al. LMO2-associated clonal T cell proliferation in two patients after gene therapy for SCID-X1. Science 302, 415–419 (2003).
68. Macchiarulo, E., Bassett, P. & Dudley, M. Challenges and progress in lentiviral vector bioprocessing. Cell Gene Ther. Insights 4, 915–923 (2018).
69. Berkhout, B. A Fourth Generation Lentiviral Vector: Simplifying Genomic Gymnastics. Mol. Ther. J. Am. Soc. Gene Ther. 25, 1741–1743 (2017).
70. Kohn, D. B., Chen, Y. Y. & Spencer, M. J. Successes and challenges in clinical gene therapy. Gene Ther. 30, 738–746 (2023).
71. Shui, S., Wang, S. & Liu, J. Systematic Investigation of the Effects of Multiple SV40 Nuclear Localization Signal Fusion on the Genome Editing Activity of Purified SpCas9. Bioeng. Basel Switz. 9, 83 (2022).

72. Kim, S., Kim, D., Cho, S. W., Kim, J. & Kim, J.-S. Highly efficient RNA-guided genome editing in human cells via delivery of purified Cas9 ribonucleoproteins. Genome Res. 24, 1012–1019 (2014).

73. Yin, H., Kauffman, K. J. & Anderson, D. G. Delivery technologies for genome editing. Nat. Rev. Drug Discov. 16, 387–399 (2017).

74. Pardi, N., Hogan, M. J., Porter, F. W. & Weissman, D. mRNA vaccines — a new era in vaccinology. Nat. Rev. Drug Discov. 17, 261–279 (2018).

75. Finn, J. D. et al. A Single Administration of CRISPR/Cas9 Lipid Nanoparticles Achieves Robust and Persistent In Vivo Genome Editing. Cell Rep. 22, 2227–2235 (2018).

76. Semple, S. C. et al. Rational design of cationic lipids for siRNA delivery. Nat. Biotechnol. 28, 172–176 (2010).

77. Mangeot, P. E. et al. Genome editing in primary cells and in vivo using viral-derived Nanoblades loaded with Cas9-sgRNA ribonucleoproteins. Nat. Commun. 10, 45 (2019).

78. Banskota, S. et al. Engineered virus-like particles for efficient in vivo delivery of therapeutic proteins. Cell 185, 250-265.e16 (2022).

79. Raguram, A., Banskota, S. & Liu, D. R. Therapeutic in vivo delivery of gene editing agents. Cell 185, 2806–2827 (2022).

80. Foss, D. V. et al. Peptide-mediated delivery of CRISPR enzymes for the efficient editing of primary human lymphocytes. Nat. Biomed. Eng. 7, 647–660 (2023).

81. Sahu, S. U. et al. Peptide-enabled ribonucleoprotein delivery for CRISPR engineering (PERC) in primary human immune cells and hematopoietic stem cells. Nat. Protoc. (2025) doi:10.1038/s41596-025-01154-8.

82. Shahbazi, R. et al. Targeted homology-directed repair in blood stem and progenitor cells with CRISPR nanoformulations. Nat. Mater. 18, 1124–1132 (2019).
83. Dykman, L. A. & Khlebtsov, N. G. Gold nanoparticles in biology and medicine: recent advances and prospects. Acta Naturae 3, 34–55 (2011).
84. Dreaden, E. C., Alkilany, A. M., Huang, X., Murphy, C. J. & El-Sayed, M. A. The golden age: gold nanoparticles for biomedicine. Chem. Soc. Rev. 41, 2740–2779 (2012).
85. Lee, K. et al. Nanoparticle delivery of Cas9 ribonucleoprotein and donor DNA in vivo induces homology-directed DNA repair. Nat. Biomed. Eng. 1, 889–901 (2017).
86. Mout, R. et al. Direct Cytosolic Delivery of CRISPR/Cas9-Ribonucleoprotein for Efficient Gene Editing. ACS Nano 11, 2452–2458 (2017).
87. Lee, Y.-W. et al. In Vivo Editing of Macrophages through Systemic Delivery of CRISPR-Cas9-Ribonucleoprotein-Nanoparticle Nanoassemblies. Adv. Ther. 2, 1900041 (2019).
88. Morgan, R. A., Gray, D., Lomova, A. & Kohn, D. B. Hematopoietic Stem Cell Gene Therapy: Progress and Lessons Learned. Cell Stem Cell 21, 574–590 (2017).
89. Shirley, J. L., De Jong, Y. P., Terhorst, C. & Herzog, R. W. Immune Responses to Viral Gene Therapy Vectors. Mol. Ther. 28, 709–722 (2020).
90. Xue, Y., Li, X., Li, H. & Zhang, W. Quantifying thiol–gold interactions towards the efficient strength control. Nat. Commun. 5, 4348 (2014).
91. Neuberg, P. & Kichler, A. Recent developments in nucleic acid delivery with polyethylenimines. Adv. Genet. 88, 263–288 (2014).
92. Santos, L. et al. Comparison of Cas9 and Cas12a CRISPR editing methods to correct the W1282X-CFTR mutation. J. Cyst. Fibros. 21, 181–187 (2022).

93. Chen, W. et al. Massively parallel profiling and predictive modeling of the outcomes of CRISPR/Cas9-mediated double-strand break repair. Nucleic Acids Res. 47, 7989–8003 (2019).

94. Pinello, L. et al. Analyzing CRISPR genome-editing experiments with CRISPResso. Nat. Biotechnol. 34, 695–697 (2016).

95. Zerulla, D., Uhlig, I., Szargan, R. & Chassé, T. Competing interaction of different thiol species on gold surfaces. Surf. Sci. 402–404, 604–608 (1998).

96. O'Reilly, D. et al. Extensive CRISPR RNA modification reveals chemical compatibility and structure-activity relationships for Cas9 biochemical activity. Nucleic Acids Res. 47, 546–558 (2019).

97. Merdan, T. et al. PEGylation of poly(ethylene imine) affects stability of complexes with plasmid DNA under in vivo conditions in a dose-dependent manner after intravenous injection into mice. Bioconjug. Chem. 16, 785–792 (2005).

98. Jiang, Y. et al. Quantitating Endosomal Escape of a Library of Polymers for mRNA Delivery. Nano Lett. 20, 1117–1123 (2020).

99. Zetsche, B. et al. Cpf1 is a single RNA-guided endonuclease of a class 2 CRISPR-Cas system. Cell 163, 759–771 (2015).

100. Cost, G. J. et al. A Novel Type V CRISPR System with Potential for Genome Editing in the Liver. Blood 138, 1862–1862 (2021).

101. Chen, K. et al. Lung and liver editing by lipid nanoparticle delivery of a stable CRISPR–Cas9 ribonucleoprotein. Nat. Biotechnol. (2024) doi:10.1038/s41587-024-02437-3.

102. Turkevich, John, Peter Cooper Stevenson, and James Hillier. 'A study of the nucleation and growth processes in the synthesis of colloidal gold.' Discussions of the faraday society 11 (1951): 55-75.

103. Tatiossian, K. J. et al. Rational Selection of CRISPR-Cas9 Guide RNAs for Homology-Directed Genome Editing. Mol. Ther. J. Am. Soc. Gene Ther. 29, 1057–1069 (2021).

104. Bloomer, H., Khirallah, J., Li, Y. & Xu, Q. CRISPR/Cas9 ribonucleoprotein-mediated genome and epigenome editing in mammalian cells. Adv. Drug Deliv. Rev. 181, 114087 (2022).

105. Raguram, A., An, M., Chen, P. Z. & Liu, D. R. Directed evolution of engineered virus-like particles with improved production and transduction efficiencies. Nat. Biotechnol. (2024) doi:10.1038/s41587-024-02467-x.

106. Rix, B., Maduro, A. H., Bridge, K. S. & Grey, W. Markers for human haematopoietic stem cells: The disconnect between an identification marker and its function. Front. Physiol. 13, 1009160 (2022).

107. Berckmueller, K. et al. CD90-targeted lentiviral vectors for HSC gene therapy. Mol. Ther. 31, 2901–2913 (2023).

108. Cannon, P. et al. Safe and Effective In Vivo Targeting and Gene Editing in Hematopoietic Stem Cells: Strategies for Accelerating Development. Hum. Gene Ther. 32, 31–42 (2021).

109. Shi, D., Toyonaga, S. & Anderson, D. G. In Vivo RNA Delivery to Hematopoietic Stem and Progenitor Cells via Targeted Lipid Nanoparticles. Nano Lett. 23, 2938–2944 (2023).

110. Wojnilowicz, M., Glab, A., Bertucci, A., Caruso, F. & Cavalieri, F. Super-resolution Imaging of Proton Sponge-Triggered Rupture of Endosomes and Cytosolic Release of Small Interfering RNA. ACS Nano 13, 187–202 (2019).

111. Luk, K. et al. Optimization of Nuclear Localization Signal Composition Improves CRISPR-Cas12a Editing Rates in Human Primary Cells. GEN Biotechnol. 1, 271–284 (2022).

112. Hamaly, M. A., Abulateefeh, S. R., Al-Qaoud, K. M. & Alkilany, A. M. Freeze-drying of monoclonal antibody-conjugated gold nanorods: Colloidal stability and biological activity. Int. J. Pharm. 550, 269–277 (2018).